# Semileptonic B Decays from an NRQCD/D234 Action

 $J.Shigemitsu^a$ ,  $S.Collins^b$ ,  $C.T.H.Davies^b$ ,  $J.Hein^c$ ,  $R.R.Horgan^d$ ,  $G.P.Lepage^e$ .

<sup>a</sup>Physics Department, The Ohio State University, Columbus, OH 43210, USA.
 <sup>b</sup>Department of Physics & Astronomy, University of Glasgow, Glasgow, G12 8QQ, UK.
 <sup>c</sup>Department of Physics & Astronomy, University of Edinburgh, Edinburgh, EH9 3JZ, UK.
 <sup>d</sup>D.A.M.T.P., CMS, Wilberforce Road, Cambridge, England CB3 0WA, UK.
 <sup>e</sup>Newman Laboratory of Nuclear Studies, Cornell University, Ithaca, NY 14853, USA.

# Abstract

Semileptonic,  $B \to \pi \ l \overline{\nu}$ , decays are studied on quenched anisotropic lattices using tree-level tadpole improved Symanzik glue, NRQCD heavy quark and D234 light quark actions. Constrained fitting methods are applied to extract groundstate contributions to two-point and three-point correlators. We agree with previous lattice determinations of the form factors. The major source of systematic error here, as in previous work, comes from the chiral extrapolation to the physical pion mass. Future calculations must work at lighter quark masses to resolve this.

PACS numbers: 12.38.Gc, 13.20.He, 14.40.Nd

#### I. INTRODUCTION

Determinations of the CKM matrix element  $|V_{ub}|$  from exclusive semileptonic B decays rely on lattice input for the  $\langle \pi | J_{\mu} | B \rangle$  or  $\langle \rho | J_{\mu} | B \rangle$  matrix elements. Reducing errors in these lattice calculations and extending their kinematic range will be an important contribution to consistency tests of the CKM matrix, and thereby of the Standard Model. Several quenched studies of  $B \to \pi l \overline{\nu}$  decays have been carried out in recent years employing a wide range of different actions and methods [1–4]. Despite the differences in sources of systematic errors there is general agreement in final results, especially for the form factor  $f_+(q^2)$  which is directly relevant for the differential decay rate measured in experiments.

The difficulties with lattice simulations for these semileptonic form factors are well known. Lattice calculations are most reliable at large  $q^2 \equiv (p_{\pi} - p_B)^2$ , i.e. close to the zero recoil point, whereas experiments are limited to smaller  $q^2$ . In the B meson rest frame, small  $q^2$  implies large pion momenta which introduces both  $ap_{\pi}$  discretization errors on the lattice and large statistical errors. Furthermore it is becoming increasingly more evident that a major source of systematic error comes from the chiral extrapolation to a physical final state pion.

This article describes further investigations of  $B \to \pi l \overline{\nu}$  decays in the quenched approximation, where we have experimented with ways to improve errors due to finite pion momenta. The first difference from previous work is the use of more highly improved actions. We employ Symanzik glue rather than the Wilson glue action, the D234 light quark action rather than clover and an NRQCD action corrected through  $O(a^2)$ . We find good dispersion relations for pion energies up to at least 1.5GeV. The ability or inability to cover a  $q^2$  range overlapping with experiment is determined more by the other challenges, namely statistical noise and chiral extrapolations, than by discretization errors. This will be even more true if one goes to lattices finer than the relatively coarse,  $1/a_s = 1.2 \text{GeV}$ , lattices used in the present study.

The other two new ingredients here are the use of an anisotropic lattice and constrained fitting methods. As demonstrated in many contexts, anisotropic lattices lead to correlators that have a larger number of data points inside the time region where signal-to-noise is still good. This allows for more accurate extraction of energies and amplitudes [5–8]. Reference [8] showed the advantages of anisotropic lattices for correlators involving finite momentum hadrons. In the present work we add one more major improvement to this scheme, namely constrained fits [9]. These new analysis tools, based on Bayesian statistics, allow us to increase the number of exponentials in fits to single correlators, without losing stability or having errors in low lying energies become large. One typically fits to all (or almost all) data points, with  $t_{min} = 0$  or = 1, irrespective of where or whether a plateau sets in. Hence one can take full advantage of all the data points with small statistical errors that the anisotropic lattice gives us. Previously if one just went to anisotropic lattices and used conventional fitting methods one had to rely on having excellent smearings or a large matrix of smearings to ensure overlap between a plateau region and the region with good signal-to-noise.

We find that constrained fits allow us to extract groundstate contributions to two-point and three-point correlators in a controlled way despite the fact that our smearings are far from optimal. Nevertheless, our final results for  $B \to \pi \ l\overline{\nu}$  form factors still exhibit large systematic errors, comparable to those quoted by other groups. The main reason for this is that our systematic error is dominated by the chiral extrapolation uncertainties. The D234 light quark action suffers, in common with the clover and Wilson actions, from exceptional configurations. This limits our ability to go to small pion masses and necessitates a large chiral extrapolation (we work in the range  $0.7m_{strange} < m_q < 1.3m_{strange}$ ). Even the correct ansatz for the extrapolation is unclear at the present time. In the future, rather than try to go to finer lattices with the same action, we believe that, in order to improve on chiral extrapolation errors, one needs to go to light quark actions with good chiral properties. Work with improved staggered light quarks, for instance, has already started [10,11].

Difficulties with chiral extrapolations also limit our ability to go to pion energies larger than 1 GeV (or  $q^2 < 16 \text{GeV}^2$ ). If one were to work harder and double the statistics one might be able to consider pions with momenta up to 1.5 GeV and go down to  $q^2 \sim 12 \text{Gev}^2$  as long as the light quark mass stays around the strange mass. Nevertheless, carrying out chiral extrapolations at large pion momenta would introduce prohibitively large errors. Recently the idea has been put forward of working in a reference frame where the entire  $q^2$  range can be covered with pions having momenta less than 1 GeV (see ref. [12] for discussion of the "Moving NRQCD" formalism). We believe the future of accurate semileptonic B decay studies lies in a combination of using light quark actions with good chiral properties and a formalism that can handle B mesons decaying at large velocities. The lessons derived from the present project should be very useful in such future work, especially in the analysis of three-point correlators.

In the next section we introduce the actions used in this project. Section III provides simulation details and discusses results from two-point correlators. Section IV describes our direct fits to three-point correlators. This step replaces the conventional approach of considering ratios of three- and two-point correlators and looking for a plateau which is then fit to a constant. In section V we discuss chiral extrapolations and present results for form factors. Comparisons are made with previous lattice work. We then conclude with a summary section. We delegate details of constrained fitting methods to an appendix. A further appendix lists heavy-light current one-loop matching coefficients for the action used in this article.

### II. GAUGE AND QUARK ACTIONS

The gauge and quark actions of this article are the anisotropic actions discussed in ref. [8]. For the glue we use the tree-level tadpole-improved Symanzik action with rectangles only in spatial directions.

$$S_G = -\beta \sum_{x,s>s'} \frac{1}{\chi_0} \left\{ \frac{5}{3} \frac{P_{ss'}}{u_s^4} - \frac{1}{12} \frac{R_{ss'}}{u_s^6} - \frac{1}{12} \frac{R_{s's}}{u_s^6} \right\} -\beta \sum_{x,s} \chi_0 \left\{ \frac{4}{3} \frac{P_{st}}{u_s^2 u_t^2} - \frac{1}{12} \frac{R_{st}}{u_s^4 u_t^2} \right\}.$$
 (1)

 $P_{\mu\nu}$  and  $R_{\mu\nu}$  denote plaquettes and rectangles in the  $\mu\nu$  plane. The variables s and s' run only over spatial directions and  $u_t$  and  $u_s$  are the tadpole-improvement " $u_0$ " factors for temporal and spatial link variables respectively. We use the Landau link definition of  $u_0$  in this article.  $\chi_0$  is the bare anisotropy which differs from the true or renormalized anisotropy,

$$\chi \equiv a_s/a_t,\tag{2}$$

in the presence of quantum corrections. We use torelon dispersion relations [13] to fix  $\chi$  nonperturbatively. Starting with  $\chi_0 = 3$ . at  $\beta = 2.4$  we find the renormalized anisotropy to be  $\chi = 2.71(3)$ .

The light quark action is the D234 action of ref. [14] modified for anisotropic lattices.

$$S_{D234}^{(aniso)} = a_s^3 a_t \sum_x \overline{\Psi}_c \left\{ \gamma_t \frac{1}{a_t} \nabla_t + \frac{C_0}{a_s} \vec{\gamma} \cdot (\vec{\nabla} - \frac{1}{6} C_3 \vec{\nabla}^{(3)}) + m_0 - \frac{r a_s}{2} \left[ \frac{1}{a_t^2} \nabla_t^{(2)} + \frac{1}{a_s^2} \sum_{j=1}^3 (\nabla_j^{(2)} - \frac{1}{12} C_4 \nabla_j^{(4)}) \right] - r a_s \frac{C_F}{4} \frac{i \sigma_{\mu\nu} \tilde{F}^{\mu\nu}}{a_\mu a_\nu} \right\} \Psi_c$$

$$= \sum_x \overline{\Psi} \left\{ \gamma_t \nabla_t + \frac{C_0}{\chi} \vec{\gamma} \cdot (\vec{\nabla} - \frac{1}{6} C_3 \vec{\nabla}^{(3)}) + a_t m_0 - \frac{r}{2} \left[ \chi \nabla_t^{(2)} + \frac{1}{\chi} \sum_{j=1}^3 (\nabla_j^{(2)} - \frac{1}{12} C_4 \nabla_j^{(4)}) \right] - r \frac{C_F}{4} i \sigma_{\mu\nu} \tilde{F}^{\mu\nu} \frac{a_s a_t}{a_\mu a_\nu} \right\} \Psi$$

$$(4)$$

The quark fields  $\Psi_c$  and the dimensionless lattice fields  $\Psi$  are related through

$$\Psi = a_s^{3/2} \Psi_c. \tag{5}$$

Definitions of lattice derivatives and the improved  $\tilde{F}_{\mu\nu}$  are given, for instance, in the appendix to ref. [15]. We work with r,  $C_F$ ,  $C_3$  and  $C_4$  all set equal to one. The "speed of light" coefficient,  $C_0$ , is tuned perturbatively or nonperturbatively using pion dispersion relations. Its actual value will be discussed in the next section.

For the heavy quark we use the standard NRQCD evolution equations which follow from the action [16,17],

$$S_{NRQCD} = \sum_{x} \left\{ \overline{\Phi}_{t} \Phi_{t} - \overline{\Phi}_{t} \left( 1 - \frac{a_{t} \delta H}{2} \right)_{t} \left( 1 - \frac{a_{t} H_{0}}{2n} \right)_{t}^{n} U_{4}^{\dagger} \left( 1 - \frac{a_{t} H_{0}}{2n} \right)_{t-1}^{n} \left( 1 - \frac{a_{t} \delta H}{2} \right)_{t-1} \Phi_{t-1} \right\}.$$
 (6)

 $H_0$  is the nonrelativistic kinetic energy operator,

$$a_t H_0 = -\frac{\Delta^{(2)}}{2\chi(a_s M_0)},\tag{7}$$

and  $\delta H$  includes 1/M relativistic and  $O(a^2)$  finite lattice spacing corrections,

$$a_t \delta H = -\frac{1}{2\chi(a_s M_0)} \boldsymbol{\sigma} \cdot \tilde{\mathbf{B}} + \frac{\Delta^{(4)}}{24\chi(a_s M_0)}.$$
 (8)

All derivatives are tadpole improved and,

$$\Delta^{(2)} = \sum_{j=1}^{3} \nabla_j^{(2)}, \qquad \Delta^{(4)} = \sum_{j=1}^{3} \nabla_j^{(4)}$$
 (9)

The leading discretization errors in the total action are  $O(a_s \alpha_s)$  errors coming from the light quark action. The leading relativistic corrections are  $O(\alpha_s \frac{\Lambda_{QCD}}{M})$  coming from one-loop corrections to tree-level coefficients in the NRQCD action. We will work with heavy-light currents corrected to the same level as the action, i.e. we will include  $O(\alpha_s)$  and  $O(\Lambda_{QCD}/M)$  terms but not  $O(a_s \alpha_s)$  or  $O(\alpha_s \frac{\Lambda_{QCD}}{M})$  corrections. We estimate systematic errors from the latter terms to be at the 8% and 3% levels respectively.

#### III. SIMULATION DETAILS

Table I summarizes lattice and action parameters. We work on  $12^3 \times 48$  quenched anisotropic lattices with  $\chi \equiv a_s/a_t = 2.71(3)$ , as determined from torelon dispersion relations in the pure glue theory. We use a total of 199 configurations and run both time-forward and time-reversed NRQCD evolutions in order to increase statistics. The former uses timeslices 0-23, and the latter timeslices 0,47,46 ....25. For the *B* meson correlators and the three-point correlators we find little evidence for correlations between the two runs and close to a  $\sqrt{2}$  improvement in statistics. Nevertheless, in our data analysis we always bin the data from the two time evolutions before carrying out fits.

Based on string tension calculations we estimate the spatial lattice spacing to correspond to  $1/a_s = 1.20(5)$  GeV. The  $\rho$  mass gives a similar value of  $(1/a_s)_{\rho} = 1.18(6)$  GeV.

We have carried out simulations at five values of the bare light quark mass corresponding to P/V = 0.624(13), 0.675(8), 0.714(14), 0.736(6) and 0.760(6). In terms of  $a_t m \equiv a_t(m_0 - m_{crit.})$ , we have the range  $a_t m = 0.023$ , 0.028, 0.033, 0.038 and 0.043. The middle value of  $a_t m = 0.033$  is very close to the strange quark mass as determined by the  $\phi$ . We find  $M_V = 1.003(20)(40) \text{GeV}$  (second error comes from the uncertainty in scale which we take from the string tension) compared to the experimental  $M_{\phi} = 1.019 \text{GeV}$ . Hence our light quark masses span roughly the range from  $0.7m_s$  to  $1.3m_s$ . Clearly one would ideally like to go to much smaller quark masses. For our lightest mass we encountered one exceptional configuration in an ensemble of initially 200 configurations. This stopped us from attempting to further decrease the quark mass and reduced the number of usable configurations to 199. For the heavy quark mass we employed one value  $a_s M_0 = 4$ , tuned to be close to the b quark mass using the  $B_s$  meson mass as experimental input. Fig.1 shows  $a_t M_{kin}$  for the  $B_s$  meson extracted from B correlators with different spatial momenta.

$$M_{kin} = \frac{p^2 - \delta E(p)^2}{2 \,\delta E(p)} \tag{10}$$

with  $\delta E(p) = E_B(p) - E_B(0)$ .  $E_B$  denotes the falloff energy of B correlators and differs from the total energy of the B meson since the NRQCD action does not include a rest mass term.

This distinction is irrelevant for the difference  $E_B(p) - E_B(0)$ . Data from different momenta all give results consistent with the experimental value for  $M_{B_s}$  and also with perturbative expectations. The latter is based on

$$M_{kin}^{pert} = Z_m M_0 - E_0 + E_B(0). (11)$$

The full horizontal line in Fig.1 gives the one-loop result for  $a_t M_{kin}^{pert}$ . The two dotted lines are estimates of errors due to higher order corrections. In ref. [2] it was found that semileptonic form factors in the b quark region are not very sensitive to the heavy quark mass. Hence we believe errors coming from inadequate tuning of  $a_s M_0$  are small compared to our other systematic errors.

The "speed of light" coefficient  $C_0$  in the light quark action, eq.(4), was fixed using pion dispersion relations. We found it sufficient to consider the lowest pion momentum at one value of the bare mass ( $a_t m = 0.033$ ). This fixed  $C_0 = 0.94$  which works well for all 5 light quark masses. Fig.2 shows the speed of light C(p) defined as,

$$C(p) = \sqrt{\frac{E_{\pi}^{2}(p) - E_{\pi}^{2}(0)}{p^{2}}}$$
 (12)

for three different light quark masses. One sees that the relativistic dispersion relation holds well, within errors, for momenta up to at least 1.5GeV. In our analysis of three-point correlators and extraction of form factors we will use continuum relativistic formulas for  $E_{\pi}(p)$ . In this work it was fairly painless to fix  $C_0$  nonperturbatively. Had we used one-loop perturbation theory [15] we would not have been too far off with  $C_0^{1-loop} = 0.91(3)$ . Once two-loop results are known, we will probably be able to dispense with nonperturbative tunings of parameters such as  $C_0$  or the renormalized anisotropy  $\chi$  and anisotropic actions will be just as easy to handle as isotropic ones [18].

For completeness we show chiral extrapolations for  $m_{\rho}$  and  $E_B(0)$  in Fig.3. This leads to the  $(1/a_s)_{\rho}$  quoted above and to a  $B_s - B_d$  splitting of 86(13)MeV. The experimental  $B_s - B_d$  mass difference is 90.2(2.2)MeV.

### IV. ANALYSIS OF THREE-POINT CORRELATORS

The first step in semileptonic B decay simulations on the lattice is to calculate the three-point correlator,

$$C_{\mu}^{(3)}(\vec{p}_B, \vec{p}_{\pi}, t_B, t) = \sum_{\vec{x}} \sum_{\vec{y}} e^{-i\vec{p}_B \cdot \vec{x}} e^{i(\vec{p}_B - \vec{p}_{\pi}) \cdot \vec{y}} \langle 0 | \Phi_B(t_B, \vec{x}) V_{\mu}^L(t, \vec{y}) \Phi_{\pi}^{\dagger}(0) | 0 \rangle.$$
 (13)

 $\Phi_{\pi}^{\dagger}$  and  $\Phi_{B}^{\dagger}$  are interpolating operators used to create the pion or B meson respectively.  $V_{\mu}^{L}$  is the dimensionless Euclidean space lattice heavy-light vector current. The continuum Minkowski space  $V_{\mu}$  is related to  $V_{\mu}^{L}$  via

$$V_{\mu} = a_s^{-3} Z_{V_{\mu}} \, \xi(\mu) \, V_{\mu}^L. \tag{14}$$

 $\xi(\mu)$  is the conversion factor between Minkowski and Euclidean space  $\gamma$ -matrices and  $Z_{V_{\mu}}$  is the heavy-light current matching coefficient. Perturbative estimates of  $Z_{V_{\mu}}$  are discussed in an appendix.

We work exclusively with B mesons decaying at rest  $(\vec{p}_B = 0)$ .  $t_B$  is fixed at  $t_B = 23$  for time-forward runs and  $t_B = 25$  in time-reversed runs.

We have found it convenient to rescale  $C_{\mu}^{(3)}$  as follows,

$$\tilde{C}_{\mu}^{(3)}(p_{\pi},t) = \xi(\mu) C_{\mu}^{(3)}(\vec{p}_{B} = 0, p_{\pi}, t_{B}, t) e^{E_{B}^{(1)}(t_{B}-t)}$$
(15)

where  $E_B^{(1)}$  is the ground state B meson falloff energy, obtained from fits to two-point correlators (in a bootstrap analysis  $E_B^{(1)}$  is obtained separately for each bootstrap ensemble).  $\tilde{C}_{\mu}^{(3)}$  is then fit to,

$$\tilde{C}_{\mu}^{(3)}(p_{\pi},t) = \left\{ \sum_{j}^{N_{B}} \sum_{l}^{N_{\pi}} A_{jl} e^{-E_{\pi}^{(l)} t} e^{-E_{B}^{(j)}(t_{B}-t)} \right\} e^{E_{B}^{(1)}(t_{B}-t)} 
= \sum_{l}^{N_{\pi}} A_{1l} e^{-E_{\pi}^{(l)} t} 
+ \sum_{l}^{N'_{\pi}} A_{2l} e^{-E_{\pi}^{(l)} t} e^{-(E_{B}^{(2)} - E_{B}^{(1)})(t_{B}-t)} 
+ \dots \dots \dots$$
(16)

We use constrained (Bayesian) fits of ref. [9] to fit a single correlator to the multi-exponential form on the RHS of eq.(17). Details are given in the appendix. Fits are carried out with  $t_{min}$ fixed at  $t_{min} = 1$  and for various  $t_{max} < t_B$ . The number of exponentials is increased until a good fit to the data is obtained. For a "good fit" we generally require  $\chi^2/d.o.f. \leq 1$ . In a few cases we accept  $\chi^2/d.o.f$  as high as  $\sim 1.2$  but even in those instances the Q-values are larger than 0.2. Sample fit results for  $\langle V_0^L \rangle$  are shown in Figs.4 and 5. For pion momenta (001), (011) and (111) and using  $t_{max} = 17 \sim 21$  good fits were obtained with just the first line on the RHS of (17) and  $N_{\pi} \geq 2$ . The figures show results for  $N_{\pi} = 3$  and  $t_{max} = 19$ . For the zero momentum case an additional excited B exponential from the second line in (17) was needed for good fits with  $t_{max}$  between 17 ~ 21. Fig.4 plots the case  $N_{\pi}=3$  and  $N'_{\pi}=1$ . The fact that we can fit the data for  $t_{max}$  only slightly below  $t_B$  (the source point for the B meson) with just one or two  $E_B^{(j)}$  exponentials tells us that excited B states are highly suppressed in the three-point correlators. We believe this is a physical effect indicating that form factors for semileptonic decays of excited B mesons (proportional to  $A_{il}$  in (17) with j > 1) are suppressed relative to ground state form factors. Figs.6 and 7 show sample fits to matrix elements of the spatial component of the vector current,  $\langle V_k^L \rangle$ . Again one can go out to  $t_{max} \sim 21$  with  $N_B = 1$  for most momenta and with  $N_B = 2$  for momentum (001).

Our goal is to extract the amplitude  $A_{11}$ , the groundstate contribution to the  $C_{\mu}^{(3)}$ . From  $A_{11}$  one can then determine the B meson semileptonic decay form factors (see next section). One consistency check on  $A_{11}$  is to verify that its associated exponential factors,  $e^{-E_{\pi}^{(1)}t}e^{-E_{B}^{(1)}(t_{B}-t)}$ , involve the correct groundstate energies. For  $E_{B}$  this is put in by hand

through our rescaling in (15) and the ansatz of (17). Since we are always dealing with zero momentum B mesons for which  $E_B^{(1)}$  can be determined accurately from two-point correlators, we believe this is a sensible way to proceed. For  $E_{\pi}$ , for which we need results for various momenta, one possibility is to do simultaneous fits to two- and three-point correlators ensuring that the same set of energies appear in both correlators [19]. We have opted not to force the  $E_{\pi}^{(l)}$  in the two correlators to be equal in this way, but to do separate fits and use consistency between the two independent extractions of  $E_{\pi}^{(1)}(p)$  as a check on our fits, on our fit ansatz (17), and on our choices for  $t_{max}$ ,  $N_B$ ,  $N'_{\pi}$  etc. Fig.8 shows groundstate pion energies  $E_{\pi}(p)$  extracted from two-point and either  $\langle V_0^L \rangle$  or  $\langle V_k^L \rangle$  three-point correlators. One sees good agreement between the different determinations. One also notices that for higher momenta three-point correlators provide more accurate energies than two-point correlators. Of course, whether this happens or not depends on the smearings used in the pion interpolating operator.

In order to include  $\Lambda_{QCD}/M$  corrections to the heavy-light currents we have looked at the matrix element of

$$V_{\mu}^{(1),L} = \frac{-1}{2M_0} \, \overline{q} \gamma_{\mu} \vec{\gamma} \cdot \vec{\nabla} Q \tag{18}$$

(see ref. [20] for a complete list of 1/M current corrections). Figs. 9 and 10 show sample fits, similar to Figs.4 and 5, for  $\langle V_0^{(1),L} \rangle$ . We find that the groundstate contribution from  $V_0^{(1),L}$ is only a small fraction (1.5 -2.5%) of the leading order contribution from  $V_0^L$ . Fig.11 shows the ratio between  $A_{11}(V_0^{(1),L})$  and  $A_{11}(V_0^L)$ . We superimpose the  $O(\alpha_s/a_sM)$  power law correction that must be subtracted from the  $\langle V_0^{(1),L} \rangle$  matrix element to obtain the physical  $O(\Lambda_{OCD}/M)$  relativistic correction [21]. This is given by the full horizontal line, the dotted lines representing our estimate of uncertainties in the  $\alpha_s/a_sM$  power law subtractions. We see that the matrix element is consistent with being 100% power law. The 1/M corrections to the spatial component of the vector current,  $\langle V_k^{(1),L} \rangle$ , is found to be even smaller (at the 1% level) relative to the leading order  $\langle V_k^L \rangle$ . Since  $\langle V_k \rangle$  must be proportional to the pion momentum  $p_{\pi,k}$  (for  $\vec{p}_B = 0$ ), whereas  $V_k^{(1)}$  is sensitive mainly to the b-quark momentum inside the initial B meson at rest, one would expect  $\langle V_k^{(1),L} \rangle$  to be very small. We could not come up with a similar plausibility argument as to why the temporal component,  $\langle V_0^{(1),L} \rangle$ , should be small as well. Because the tree-level 1/M current matrix elements are so small and of the same order of magnitude as  $O(\alpha_s/a_sM)$  power law corrections, we have opted not to include them in our final analysis. Uncalculated  $O(\alpha_s^2/a_sM)$  corrections could easily switch the sign of their contributions. We are dropping terms that are 1-3\% of the leading order contributions, effects that are much smaller than the  $O(\alpha_s^2)$  systematic errors we will be assigning to the present calculation.

Our results for  $\langle V_{\mu}^{(1),L} \rangle$  disagree with those in ref. [2] where a much larger, 10 - 20%, contribution from  $V_{\mu}^{(1),L}$  is reported. The origin of this discrepancy is not understood at the present time. Nevertheless, in the next section we will see that our final results for form factors agree very well with those of ref. [2]. The global fits used there to carry out chiral extrapolations must be compensating in part for the differences in the 1/M current corrections.

#### V. RESULTS FOR FORM FACTORS

The groundstate amplitudes  $A_{11}(V_{\mu}^{L})$  extracted from fits to three-point correlators in the previous section are related to the continuum matrix element of interest as

$$\langle \pi(p_{\pi})|V^{\mu}|B(\vec{p}_{B}=0)\rangle = \frac{A_{11}(V_{\mu}^{L})}{\sqrt{\xi_{\pi}^{(1)}\xi_{B}^{(1)}}} 2\sqrt{E_{\pi}M_{B}}Z_{V_{\mu}}$$
 (19)

 $\xi_{\pi}^{(1)}$  and  $\xi_{B}^{(1)}$  are fixed from  $\pi - \pi$  and B - B correlators.

$$\sum_{\vec{x}} e^{-i\vec{p}\cdot\vec{x}} \langle 0|\Phi_{\pi}(t,\vec{x}) \Phi_{\pi}^{\dagger}(0)|0\rangle = \sum_{l} \xi_{\pi}^{(l)} \left[ e^{-E_{\pi}^{(l)}t} + e^{-E_{\pi}^{(l)}(T-t)} \right]$$
 (20)

$$\sum_{\vec{x}} \langle 0|\Phi_B(t,\vec{x})\,\Phi_B^{\dagger}(0)|0\rangle = \sum_{i} \xi_B^{(j)} e^{-E_B^{(j)}t} \tag{21}$$

The standard form factors  $f_+(q^2)$  and  $f_0(q^2)$  are defined through  $(q^\mu \equiv p_B^\mu - p_\pi^\mu)$ ,

$$\langle \pi(p_{\pi})|V^{\mu}|B(p_{B})\rangle = f_{+}(q^{2})\left[p_{B}^{\mu} + p_{\pi}^{\mu} - \frac{M_{B}^{2} - m_{\pi}^{2}}{q^{2}}q^{\mu}\right] + f_{0}(q^{2})\frac{M_{B}^{2} - m_{\pi}^{2}}{q^{2}}q^{\mu}$$
(22)

Following Fermilab [1] we have found it convenient to introduce other form factors  $f_{\parallel}$  and  $f_{\perp}$ , defined as

$$\langle \pi(p_{\pi}) | V^{\mu} | B(p_B) \rangle = \sqrt{2M_B} [v^{\mu} f_{\parallel} + p_{\perp}^{\mu} f_{\perp}].$$
 (23)

with

$$v^{\mu} = \frac{p_B^{\mu}}{M_B} \longrightarrow (1, \vec{0}) \tag{24}$$

$$p_{\perp}^{\mu} = p_{\pi}^{\mu} - E_{\pi} v^{\mu} \longrightarrow (0, \vec{p}_{\pi})$$
 (25)

 $E_{\pi}$  is the pion energy in the B meson rest frame and the last expressions in (24) and (25) are similarly the four vectors  $v^{\mu}$  and  $p_{\perp}^{\mu}$  in this frame. The form factors  $f_{\parallel}$  and  $f_{\perp}$  are useful since (again in the B rest frame) they are simply related to the three-point correlators  $C_{\mu}^{(3)}$  for  $\mu = 0$  and  $\mu = k$  respectively. One has

$$f_{\parallel} = \frac{A_{11}(V_0^L)}{\sqrt{\xi_{\pi}^{(1)}\xi_B^{(1)}}} \sqrt{2E_{\pi}} Z_{V_0}$$
 (26)

and

$$f_{\perp} = \frac{A_{11}(V_k^L)}{\sqrt{\xi_{\pi}^{(1)}\xi_B^{(1)}}} \sqrt{2E_{\pi}} Z_{V_k} / p_{\pi,k}$$
 (27)

Once  $f_{\parallel}$  and  $f_{\perp}$  are determined,  $f_{+}$  and  $f_{0}$  can then be obtained from,

$$f_{+} = \frac{1}{\sqrt{2M_B}} f_{\parallel} + \frac{1}{\sqrt{2M_B}} (M_B - E_{\pi}) f_{\perp}$$
 (28)

$$f_0 = \frac{\sqrt{2M_B}}{(M_B^2 - m_\pi^2)} \left[ (M_B - E_\pi) f_{\parallel} + (E_\pi^2 - m_\pi^2) f_{\perp} \right]$$
 (29)

From these formulas one sees that  $f_+$  will be dominated by  $f_{\perp}$ , i.e. by the matrix element of  $V_k$ , and  $f_0$  by  $f_{\parallel}$  or the matrix element of  $V_0$ .

In Fig.12 we show the form factors  $f_+$  and  $f_0$  with the light quark mass fixed at  $a_t m = 0.033$ , a value which is close to the strange quark mass. The pion momenta span (000),(001),(011),(111),(002) and (112) in units of  $2\pi/L_s a_s$ . One sees that statistical errors are reasonable down to about  $q^2 = 16 GeV^2$ . More work is required if one wants to go further away from the zero recoil point.

Figs.13 and 14 show chiral extrapolations at fixed pion momentum. We have tried linear and constant fits to either all 5 data points or to just the last 3 points. The full and dotted lines in Figs.13 and 14 give some idea of the spread in fit results. These differences are included in the chiral extrapolation systematic errors that we quote. With the present statistics it is not sensible to try more sophisticated fits. Much smaller statistical errors and data at smaller light quark masses are required to search for chiral log or square root type behavior. We also believe it is premature to try fitting to HQET and/or chiral perturbation theory inspired model ansaetze. In their plot of  $f_{\parallel}$  and  $f_{\perp}$  versus  $am_q$  the Fermilab collaboration, working at smaller quark masses than in this article, finds an upward curvature as one decreases the light quark mass [1]. We cannot rule out or verify such behavior with our present data. Fig. 15 gives form factors for the physical case  $B \to \pi l \overline{\nu}$ . One sees that errors have increased significantly over those in Fig.12. Furthermore we now include pion momenta only up to (111). Larger momenta lead to chiral extrapolation errors that are too large to make such data points meaningful.

In Fig.16 we compare our results to those by other lattice groups [1–4]. One sees that agreement for  $f_+(q^2)$  is good among all collaborations. For  $f_0(q^2)$  we agree best with the JLQCD collaboration [2] and are slightly below the results of remaining groups. The Fermilab [1] and JLQCD collaborations [2] are the two other groups that simulate directly at the b quark mass, so it is worthwhile making further comparisons with their work. We do so for the two form factors  $(f_1 + f_2)$  and  $f_2$  used by JLQCD, which are closely related to  $f_{\parallel}$  and  $f_{\perp}$ .

$$(f_1 + f_2) = \frac{1}{\sqrt{2}} f_{\parallel} , \qquad f_2 = \frac{E_{\pi}}{\sqrt{2}} f_{\perp}$$
 (30)

Figs.17 and 18 show comparisons between the three collaborations. The form factors are plotted as a function of  $E_{\pi}$ , the relation between the two variables  $q^2$  and  $E_{\pi}$  being  $q^2 = M_B^2 + m_{\pi}^2 - 2M_B E_{\pi}$ . The Fermilab results for  $(f_1 + f_2)$  are considerably higher than those from the other two collaborations. The main reason for this difference seems to come from the upward curvature, mentioned above, that Fermilab sees in their plots such as Figs.13 and 14 of form factors versus the light quark (or the pion) mass. Neither JLQCD nor the present work has sufficient accuracy at low enough quark masses to see this trend and more

calculations are required to resolve this issue. One should note that soft pion theorems, valid in the limit  $m_{\pi} \to 0$  and  $\vec{p}_{\pi} \to 0$ , would dictate

$$[f_1 + f_2]|_{E_{\pi} \to 0} = \frac{f_B}{2f_{\pi}} \sqrt{M_B}.$$
 (31)

The higher Fermilab results in Fig.17 are consistent with this relation while JLQCD's and our results are too low.

#### VI. SUMMARY

We have studied semileptonic B meson decays using highly improved gauge and quark actions on anisotropic lattices. We developed constrained fitting methods for analysing three-point correlators and extracting groundstate amplitudes in a controlled way. Our final results for form factors agree with previous lattice results.

Our data points in Figs. 16, 17 and 18 include the main systematic errors. Allowing for 8% discretization, 4% relativistic, 8% higher order perturbative and 2% mass tuning corrections, we estimate  $\sim 12\%$  systematic errors from all sources other than quenching and chiral extrapolation. This is to be compared with the 10-15% chiral extrapolation errors already shown in Fig.15. One realizes that accurate semileptonic form factor results will only be attainable if uncertainties coming from chiral extrapolations are brought under control. To overcome this obstacle, we have initiated a program to study heavy-light physics with improved staggered light quarks [11]. Simulations can be carried out with much smaller quark masses using this light quark action. The experience acquired in the present work and the analysis techniques that have been developed for three-point correlators will play an important role there. For instance, with staggered light quarks two-point and three-point correlators have time oscillating contributions which must be taken into account in fits. The only way to obtain groundstate contributions to three-point correlators will be through fitting them directly, as was done in the present article. Taking ratios of three- and two-point correlators will be of no use in simulations with staggered light quarks. Other theoretical developments, such as better understanding of chiral perturbation theory for staggered fermions [22] and the use of "Moving NRQCD" [12] should further aid accurate semileptonic form factor determinations in the future.

### **ACKNOWLEDGMENTS**

This work was supported by the DOE under DE-FG02-91ER40690 and by PPARC and NSF. Simulations were carried out at the Ohio Supercomputer Center and at NERSC. J.S. thanks the Center for Computational Physics, Tsukuba, for support and hospitality during the initial stages of this project. CTH.D. is grateful for a senior fellowship from PPARC.

#### APPENDIX A: CONSTRAINED FITTING

In this appendix we give some details of our constrained fits to two- and three-point correlators. The general approach, within the context of lattice simulations, is described in ref. [9]. In lattice simulations one typically starts with numerical data for some correlator  $\overline{G}(t)$ , averaged over configurations, which one wants to fit to a theoretical expectation  $G_{th}(t)$  to extract energies, amplitudes or matrix elements. Examples of  $G_{th}(t)$  would be the RHS's of (17), (20) or (21), which we can generically write as,

$$G_{th}(t) = \sum_{n} A_n e^{-E_n t}.$$
 (A1)

Denoting the fit parameters  $A_n$  and  $E_n$  collectively as  $\alpha_j$ , one has

$$G_{th}(t) = G_{th}(t, \{\alpha_j\}). \tag{A2}$$

Conventional fits are carried out by minimizing the  $\chi^2$ ,

$$\chi^{2}(\{\alpha_{j}\}) = \sum_{t,t'} [\overline{G(t)} - G_{th}(t, \{\alpha_{j}\})] \ \sigma_{t,t'}^{-1} \ [\overline{G(t')} - G_{th}(t', \{\alpha_{j}\})]$$
(A3)

with respect to the parameters  $\{\alpha_j\}$ .  $\sigma^{-1}$  is the inverse of the correlation matrix,

$$\sigma_{t,t'} = \overline{G(t)G(t')} - \overline{G(t)} \overline{G(t')}$$
(A4)

Depending on the quality of the data, only a few low lying energies and amplitudes will be constrained by the data. If one includes too many terms in (A1), the unconstrained  $E_n$ 's and  $A_n$ 's for higher n can wander all over the place and start to destabilize the fits.

"Constrained fits" were proposed in ref. [9] to get around this problem. One augments the conventional  $\chi^2$  with a term,  $\chi^2_{prior}$ , which prevents fit parameters that are not constrained by the data from taking on "unreasonable" unphysical values.

$$\chi^2 \longrightarrow \chi^2_{aug} \equiv \chi^2 + \chi^2_{prior},$$
(A5)

with

$$\chi_{prior}^2 \equiv \sum_j \frac{(\alpha_j - \tilde{\alpha}_j)^2}{\tilde{\sigma}_j^2}.$$
 (A6)

In this scheme each parameter  $\alpha_j$  has its set of "priors",  $\tilde{\alpha}_j$  and  $\tilde{\sigma}_j$ , and  $\chi^2_{aug}$  is designed to favor  $\alpha_j$  values in the range  $\tilde{\alpha}_j \pm \tilde{\sigma}_j$ . The replacement of eq.(A5) can be justified within the framework of Bayesian statistics and Bayes' theorem. It implies using a Gaussian apriori distribution for the parameters  $\{\alpha_j\}$ . For parameters  $\alpha_j$  that are determined by the data, adding  $\chi^2_{prior}$  has minimal effect on the final fit value, as long as  $\tilde{\sigma}_j$  is not made too small. In the present work we always set  $\tilde{\sigma}_j = \tilde{\alpha}_j$ . One is dealing with very wide Gaussians and hence very unrestrictive priors. We have checked that changing  $\tilde{\sigma}$  to 75% or 50% or even 25% of  $\tilde{\alpha}_j$  does not change results for data-determined fit parameters. Choices for the central values  $\tilde{\alpha}_j$  are made based on preliminary fits and physics input about typical level splittings in the

system under study. Again, if the  $\tilde{\sigma}_j$ 's are wide enough final results for data-determined parameters are not sensitive to precise values of the  $\tilde{\alpha}_j$ 's.

The method is best illustrated by an explicit example. Table II lists priors used in fits to pion two-point correlators for our next to lightest quark mass. Figs.19 and 20 show fit results for the groundstate energy as a function of the number of cosh's for several pion momenta. The numbers below the data points show the  $\chi^2/d.o.f.$  for the fits. The fit range is shown on the top left corner of the plots. One sees that good fits are obtained for  $N_{cosh} \geq 4$ . The fancy stars show bootstrap fit results (bootstrap methods within constrained fits are discussed below). The priors  $\tilde{E}_1$  and  $\tilde{A}_1$  and  $\tilde{E}_2$  were chosen from preliminary fits or by looking at effective mass plots. We have checked that changing them by factors of 2 moves fit results for groundstate energies and amplitudes by much less than their fit errors. (precise definition of fit errors will be given below when we discuss bootstrap methods and bootstrap errors). In Fig.21 we show what happens if one changes the priors for the higher states (n > 2) from  $[\tilde{E}_n = \tilde{E}_1 + (n-1) \times 0.3]$  to  $[\tilde{E}_1 + (n-1) \times 0.2]$ , or from  $\tilde{A}_n = 0.05$  to  $\tilde{A}_n = 0.08$ .

One sees from Figs.19 and 20 that once sufficient number of exponentials (cosh's) are included, fit results stabilize. We then fix  $N_{cosh}$  and carry out bootstrap fits for our final analysis. For instance, for pion two-point correlators we choose  $N_{cosh} = 4$ .

In a bootstrap analysis involving constrained fits one first creates a certain number (we choose nboot=200) of bootstrap ensembles in the usual way. For each bootstrap ensemble a different prior value  $\tilde{\alpha}_j$  is picked at random for each j according to a Gaussian distribution about a central value  $\tilde{\alpha}_{j,0}$  with width  $\tilde{\sigma}_j$ . In bootstrap fits, Table II should be viewed as giving values for  $\{\tilde{\alpha}_{j,0}\}$  rather than for  $\{\tilde{\alpha}_j\}$  and we set  $\tilde{\sigma}_j = \tilde{\alpha}_{j,0}$ . Fits are carried out for each of the nboot bootstrap ensembles using  $\chi^2_{aug}$  with the  $\{\tilde{\alpha}_j\}$  for that ensemble. In order to get a bootstrap average and bootstrap errors one sorts the nboot fit values according to size and discards the top and bottom 16%. We take the average of the remaining 68% as our bootstrap average and one half of the difference between the largest and smallest values within the 68% as our bootstrap error. The fancy squares in Figs.19 and 20 give bootstrap results calculated this way. One sees very good agreement between bootstrap and non-bootstrap single fits. For the latter, errors are calculated from the square root of the diagonal elements of the covariance matrix C, defined through

$$(C^{-1})_{ij} \equiv \frac{1}{2} \frac{\partial^2 \chi_{aug}^2}{\partial \alpha_i \partial \alpha_j}.$$
 (A7)

Given the very different definition of errors and the fact that in the bootstrap fits very different priors are being used compared to in the single fits (where  $\{\tilde{\alpha}_j\} \equiv \{\tilde{\alpha}_{j,0}\}$ ), we find the consistency between the two types of fits very reassuring. In Figs.22 and 23 we show fit results for the groundstate amplitudes,  $A_{11}$ , contributing to the  $\langle V_0 \rangle$  threepoint correlator (see eqns.(17) and (19) for definition of  $A_{11}$ ). The  $N_{\pi} = 3$  fits are those that went into the plots of Figs.4 and 5. One again sees good agreement between single and bootstrap fits.

#### APPENDIX B: ONE-LOOP PERTURBATIVE MATCHING

In this appendix we summarize the perturbative calculations necessary to match the NRQCD/D234 heavy-light vector current to its continuum QCD counterpart at the  $O(\alpha_s)$  and  $O(\alpha_s/a_sM)$  level. The formalism is described in detail in ref. [20]. We have generalized those calculations to include anisotropic lattices, improved glue and a more highly improved light quark action. The D234 one-loop self energy corrections have already been calculated in ref. [15] for these more complicated lattices and glue actions. In the present work we do not include  $O(a_s\alpha_s)$  or  $O(\alpha_s\frac{\Lambda_{QCD}}{M})$  terms in the action or in the currents. Hence, in the notation of ref. [20,21], only the  $\zeta_{00}$  and  $\zeta_{10}$  elements of the mixing matrix are required, in addition to the heavy quark self energy. The relation between current matrix elements  $\langle V_{\mu} \rangle$  in continuum QCD and the matrix elements  $\langle V_{\mu}^L \rangle$  evaluated on the lattice, is given to this order by,

$$\langle V_{\mu} \rangle = \frac{1}{\sqrt{Z_q^{(0)}}} \left\{ \left[ 1 + \alpha_s \tilde{\rho}_{0,\mu} \right] \langle V_{\mu}^L \rangle + \langle V_{\mu}^{(1),L} \rangle_{sub} \right\}, \tag{B1}$$

with

$$\tilde{\rho}_{0,\mu} = B_{\mu} - \frac{1}{2}(C_q + C_Q) - \zeta_{00,\mu}$$
(B2)

and

$$\langle V_{\mu}^{(1),L} \rangle_{sub} = \langle V_{\mu}^{(1),L} \rangle - \alpha_s \zeta_{10,\mu} \langle V_{\mu}^L \rangle. \tag{B3}$$

The second term proportional to  $\zeta_{10,\mu}$  is the  $O(\alpha_s/a_sM)$  power law subtraction term plotted in Fig.11.  $C_q$  and  $C_Q$  are the one-loop light and heavy quark wave function renormalizations,  $Z_q^{(0)}$  is the tree-level light quark wave function renormalization,

$$Z_q^{(0)} = \frac{1}{\sqrt{(a_t m)^2 + 2(a_t m)\chi + 1}},$$
(B4)

and  $B_{\mu}$  is given by,

$$B_0 = \frac{1}{\pi} \left[ -\frac{1}{4} + \ln(a_s M) \right], \qquad B_k = \frac{1}{\pi} \left[ -\frac{11}{12} + \ln(a_s M) \right].$$
 (B5)

In Table III we list one-loop results for  $C_q$ ,  $C_Q$ ,  $\zeta_{00,\mu}$  and  $\zeta_{10,\mu}$  for  $a_sM=4.0$  and massless light quarks. We work in general gauge ( $\alpha_g=1$  and  $\alpha_g=0$  correspond to Feynman and Landau gauges respectively) and use gauge invariance of  $\zeta_{10,\mu}$  and the combination  $[\frac{1}{2}(C_q+C_Q)+\zeta_{00,\mu}]$  as checks on our calculations. In Table III we present only the IR finite parts of  $C_q$ ,  $C_Q$  and  $\zeta_{00,\mu}$ . The IR divergent pieces cancel between the lattice and continuum parts of the matching calculation. The Landau gauge results have smaller numerical integration errors since both the light quark wave function renormalization and the heavy-light vertex correction are IR finite in this gauge.

For reasons described in the text, we do not include  $\langle V_{\mu}^{(1)} \rangle_{sub}$  in our final results. The matching factors  $Z_{V_{\mu}}$  of eqs.(19), (26) and (27) are then given by,

$$Z_{V_{\mu}} = \frac{1}{\sqrt{Z_q^{(0)}}} \left[ 1 + \alpha_s \tilde{\rho}_{0,\mu} \right]$$
 (B6)

We have used  $\alpha_s \approx 0.25(5)$  in our perturbative matching. These values are close to  $\alpha_V(2/a_s)$  estimated on isotropic lattices with unimproved glue. Systematic errors assigned to higher order perturbative corrections should cover this uncertainty in  $\alpha_s$ .

# REFERENCES

- [1] A. El-Khadra et al. [Fermilab Collaboration], Phys. Rev. **D64**:014502 (2001).
- [2] S. Aoki *et al.* [JLQCD Collaboration], Phys. Rev. **D64**:114505 (2001).
- [3] A. Abada et al. [APE Collaboration], Nucl. Phys. **B619**, 565 (2001).
- [4] K.C. Bowler et al. [UKQCD Collaboration], Phys. Lett. **B486** (2000) 111.
- [5] C. Morningstar and M. Peardon, Phys. Rev. **D60**:034509 (1999).
- [6] T. Manke et al., Phys. Rev. Lett 82:4396 (1999).
- [7] I. Drummond *et al.*, Phys. Lett. **B478**, 151 (2000).
- [8] S. Collins *et al.*, Phys. Rev. **D64**:055002 (2001).
- [9] G.P. Lepage *et al.*, Nucl. Phys. **B**(Proc. Suppl.)**106**, 12 (2002).
- [10] S. Naik, Nucl. Phys. **B316**, 238 (1989).
  - G. P. Lepage, Phys. Rev. **D59**:074501 (1999).
  - K. Orginos, D. Toussaint and R.L. Sugar, Phys. Rev. **D60**:054503 (1999).
- [11] M. Wingate et al., Nucl. Phys. B(Proc. Suppl.)106, 379 (2002);
  M. Wingate; talk presented at "Lattice 02".
- [12] K. Foley; poster presented at "Lattice 02".
- [13] M. Alford et al. Phys. Rev. **D63**:074501 (2001).
- [14] M. Alford, T. Klassen and G. P. Lepage, Phys. Rev. D58:034503 (1998), Nucl. Phys. B496 377 (1997).
- [15] S. Groote and J. Shigemitsu, Phys. Rev. **D62**:014508 (2000).
- [16] G.P. Lepage et al., Phys. Rev. **D46**, 4052 (1992).
- [17] I. Drummond et al., Nucl. Phys. **B**(Proc. Suppl.)**73**, 336 (1999).
- [18] A. Hart and R.R. Horgan; poster presented at "Lattice 02".
- [19] M. Guertler et al.; Nucl. Phys. **B**(Proc. Suppl.)**106**, 409 (2002).
- [20] C. Morningstar and J. Shigemitsu; Phys. Rev. D57, 6741 (1998); Phys. Rev. D59:094504 (1999).
- [21] S. Collins et al., Phys. Rev. **D63**:034505 (2001).
- [22] C. Bernard; talk presented at "Lattice 02".

 $\label{eq:TABLES} \mbox{TABLE I. Simulation Details.}$ 

-		
lattice size	$12^3 \times 48$	
# configs	199	
eta	2.4	
Landau link $u_0$	$u_s = 0.7868$ $u_t = 0.9771$	
$\chi_0$	3.0	
$\chi = a_s/a_t$	2.71(3)	
$C_0$	0.94	
$a_s^{-1}$	$1.20(5)  \mathrm{GeV}$	
$a_t m$	0.023 - 0.043	
P/V	0.62 - 0.76	
$a_s M_0$	4.0	

TABLE II. Priors used in pion correlators for  $a_t m = 0.028$ 

	$ ilde{E}_n =  ilde{\sigma}_{E_n}$	$\tilde{A}_n = \tilde{\sigma}_{A_n}$
$\underline{n=1}$		
mom = (000)	0.20	0.07
(001)	0.28	0.04
(011)	0.34	0.03
(111)	0.40	0.02
(002)	0.50	0.02
(112)	0.54	0.02
$\underline{n>1}$	$\tilde{E}_1 + (n-1) \times 0.3$	0.05

TABLE III. One-loop perturbative coefficients for  $a_sM=4.0$ , massless light quarks and  $\chi=2.71$ . The coefficients  $C_Q$ ,  $C_q$ ,  $\zeta_{00,\mu}$ ,  $\zeta_{10,\mu}$  and  $\tilde{\rho}_{0,\mu}$  are defined in Appendix B.  $\alpha_g$  is the gauge parameter.

	$V_0$		$V_k$	
	$\alpha_g = 1$	$\alpha_g = 0$	$\alpha_g = 1$	$\alpha_g = 0$
$C_Q \ C_q$	0.020(3)	0.520(3)		
$\zeta_{00,\mu}$	-0.066(3) 0.629(1)	0.435(1) $0.1285$	0.506(1)	0.0070
$\zeta_{10,\mu}$	-0.096	-0.096	0.054	0.054
$\frac{1}{2}(C_Q + C_q)$				
$+\zeta_{00,\mu}]$	0.606(3)	0.606(2)	0.483(3)	0.485(2)
$ ilde ho_{0,\mu}$	-0.244(3)	-0.244(2)	-0.334(3)	-0.332(2)

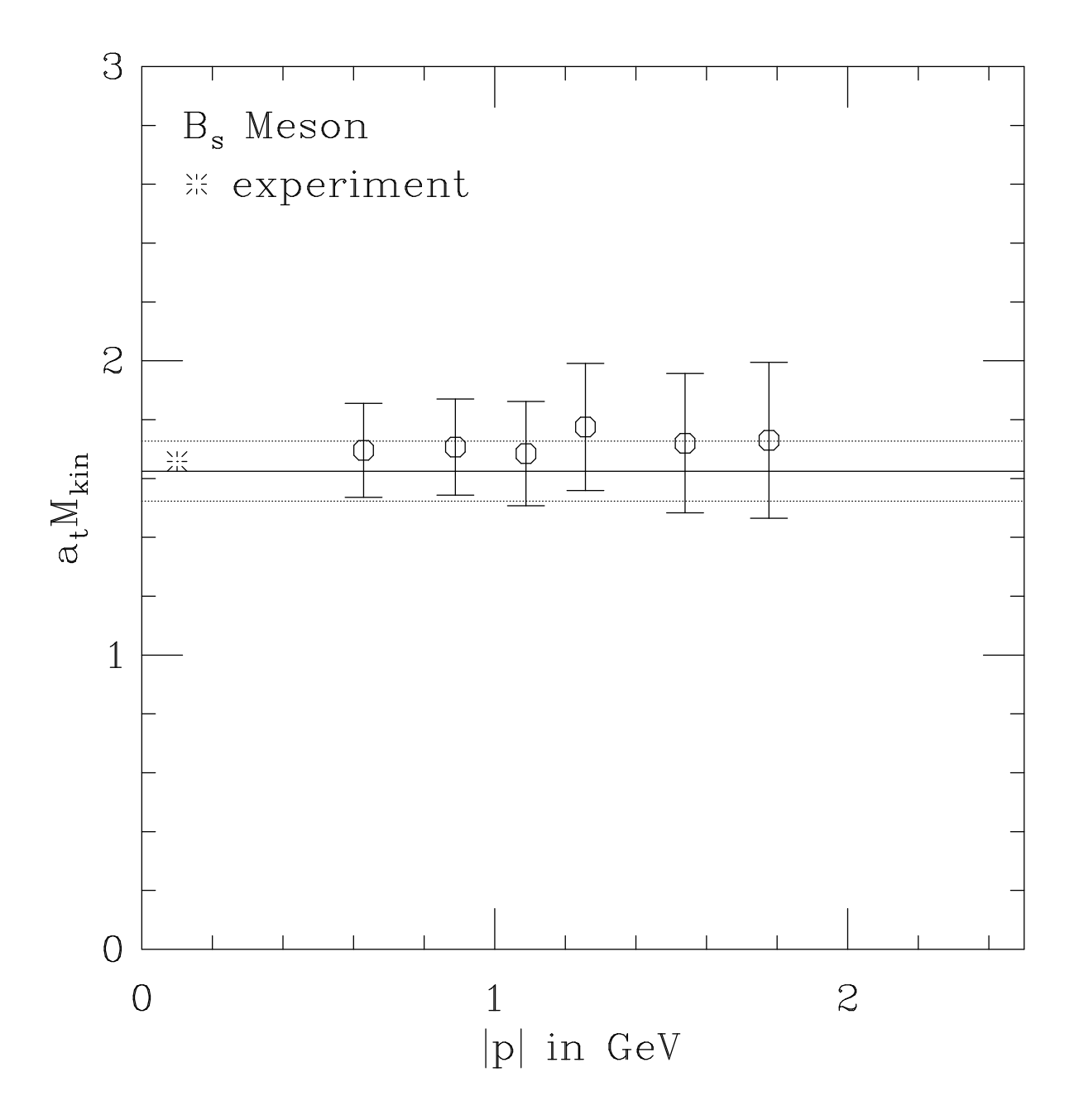


FIG. 1.  $a_t M_{kin}$  derived from correlators with different momenta. The full horizontal line gives the one-loop perturbative estimate. The two dotted horizontal lines indicate perturbative errors.

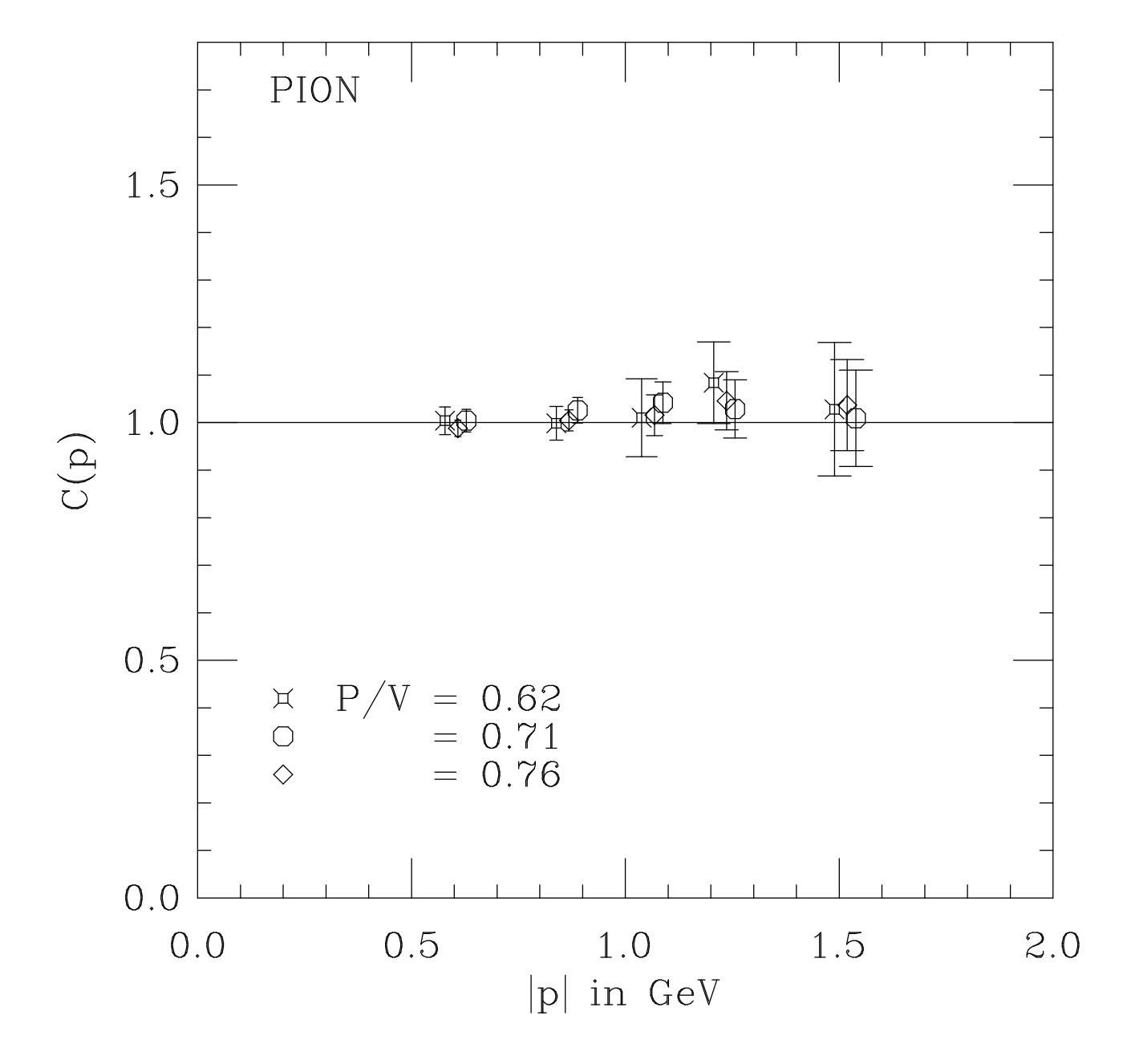


FIG. 2. C(p) versus the pion momentum for three light quark masses.

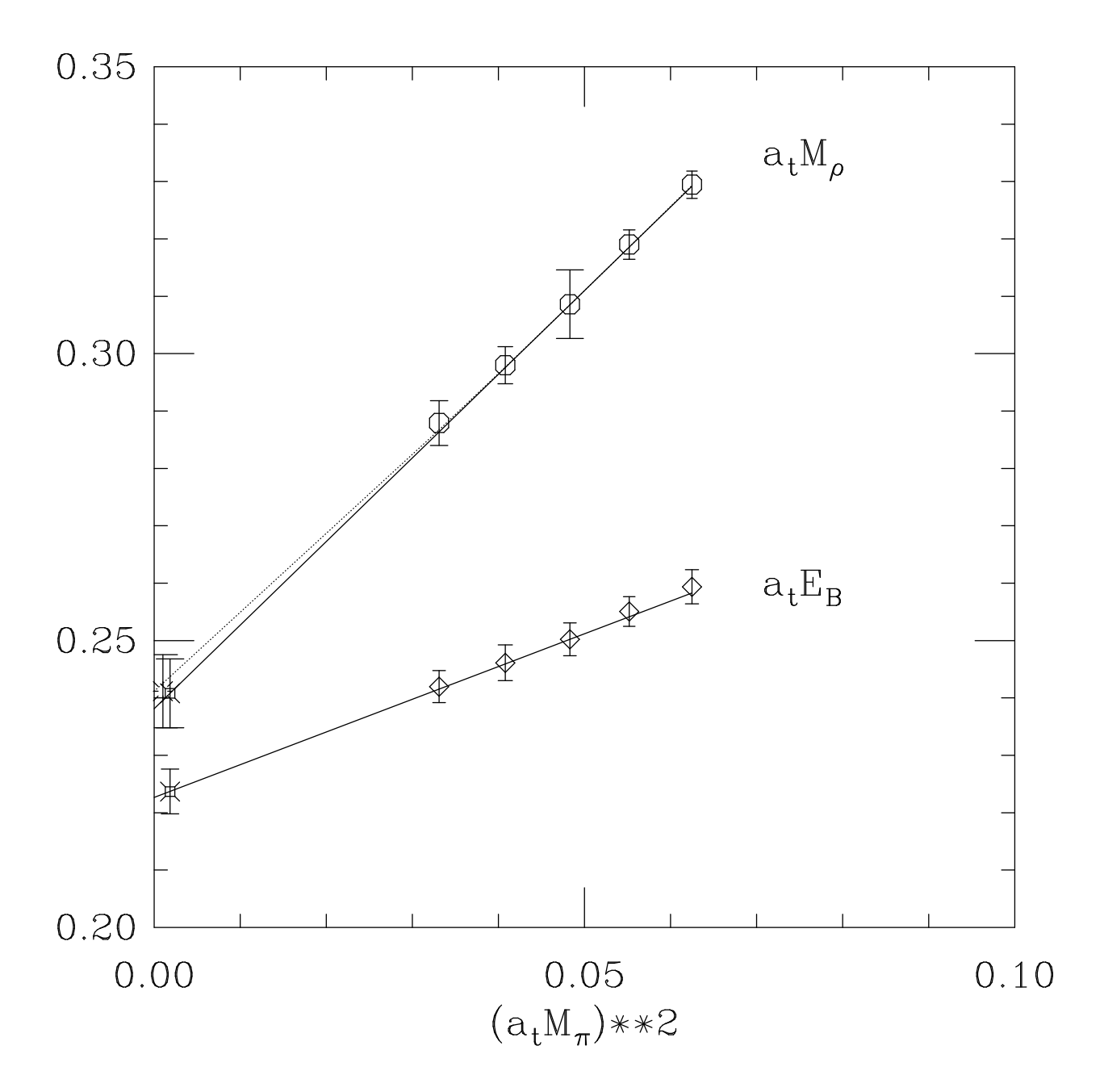


FIG. 3. Chiral extrapolation of the  $\rho$  mass and of  $E_B(0)$ . For  $a_t m_{\rho}$  both linear (full line) and quadratic (dotted line) extrapolations are shown.

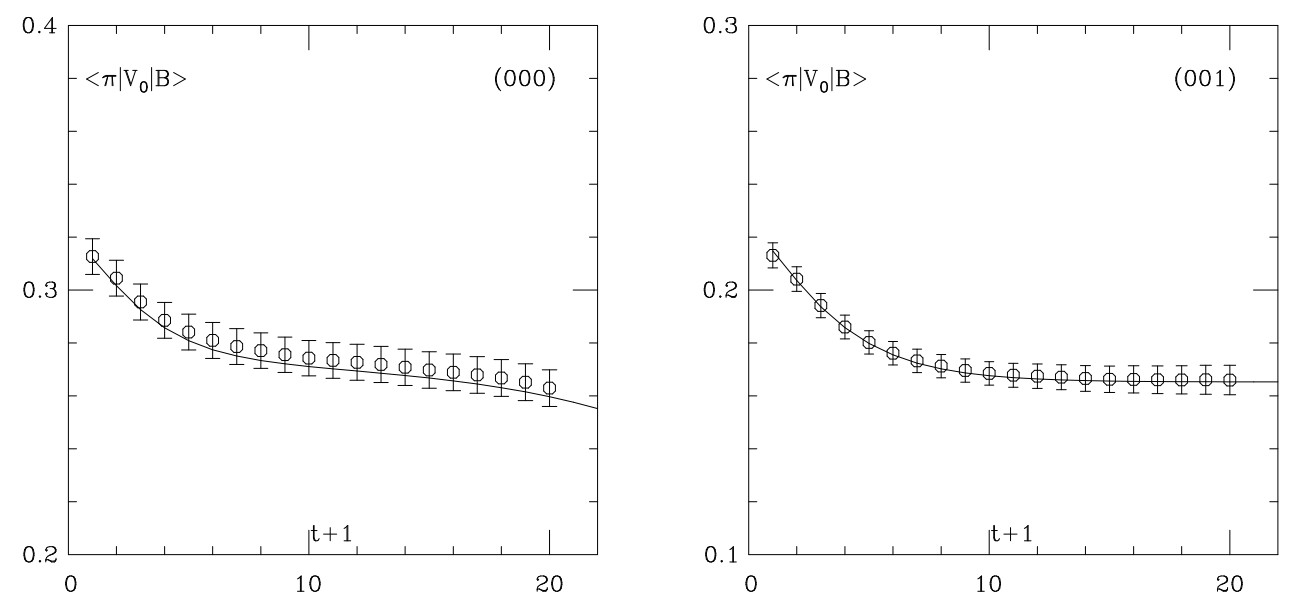
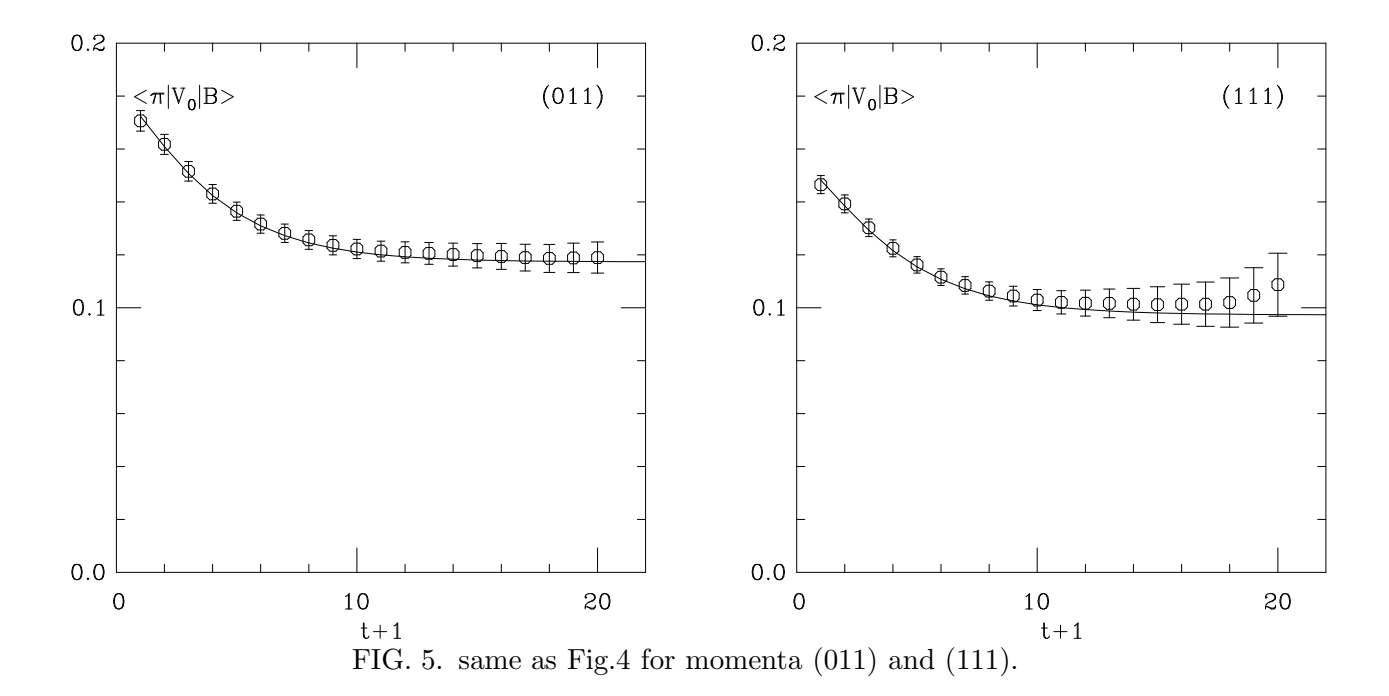
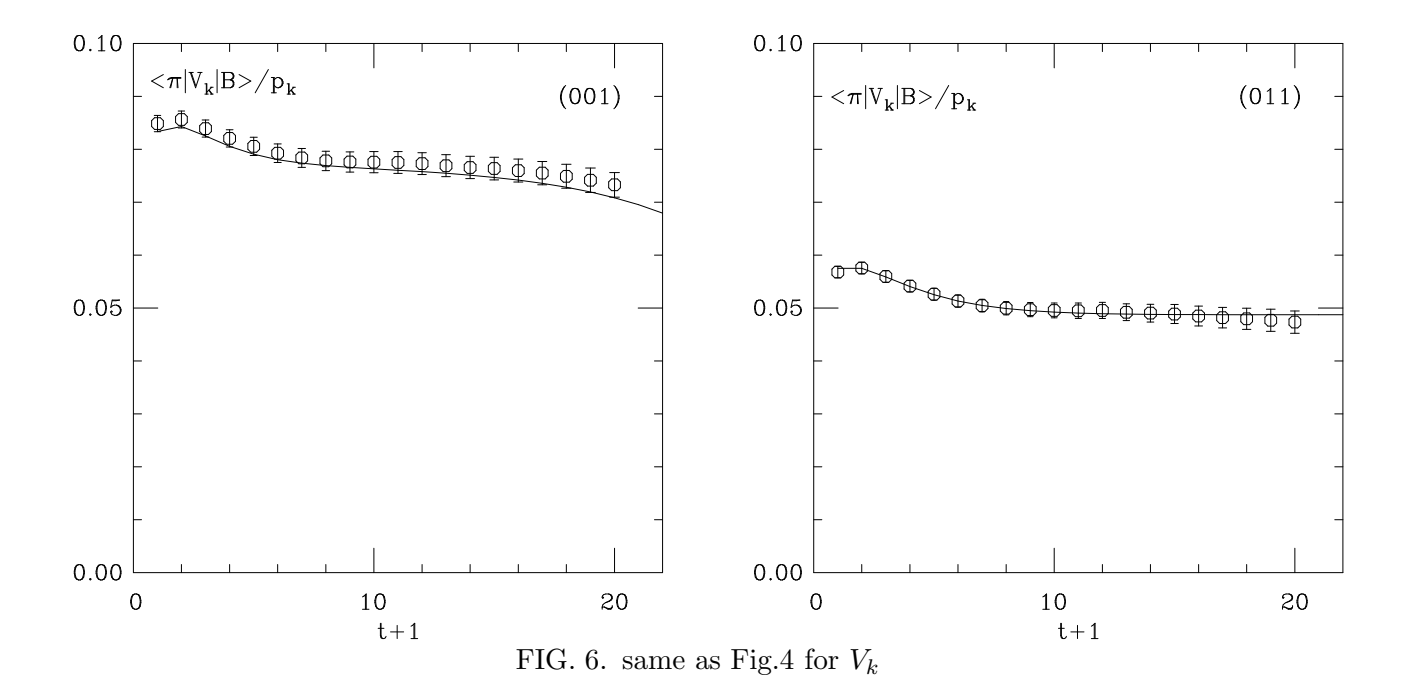
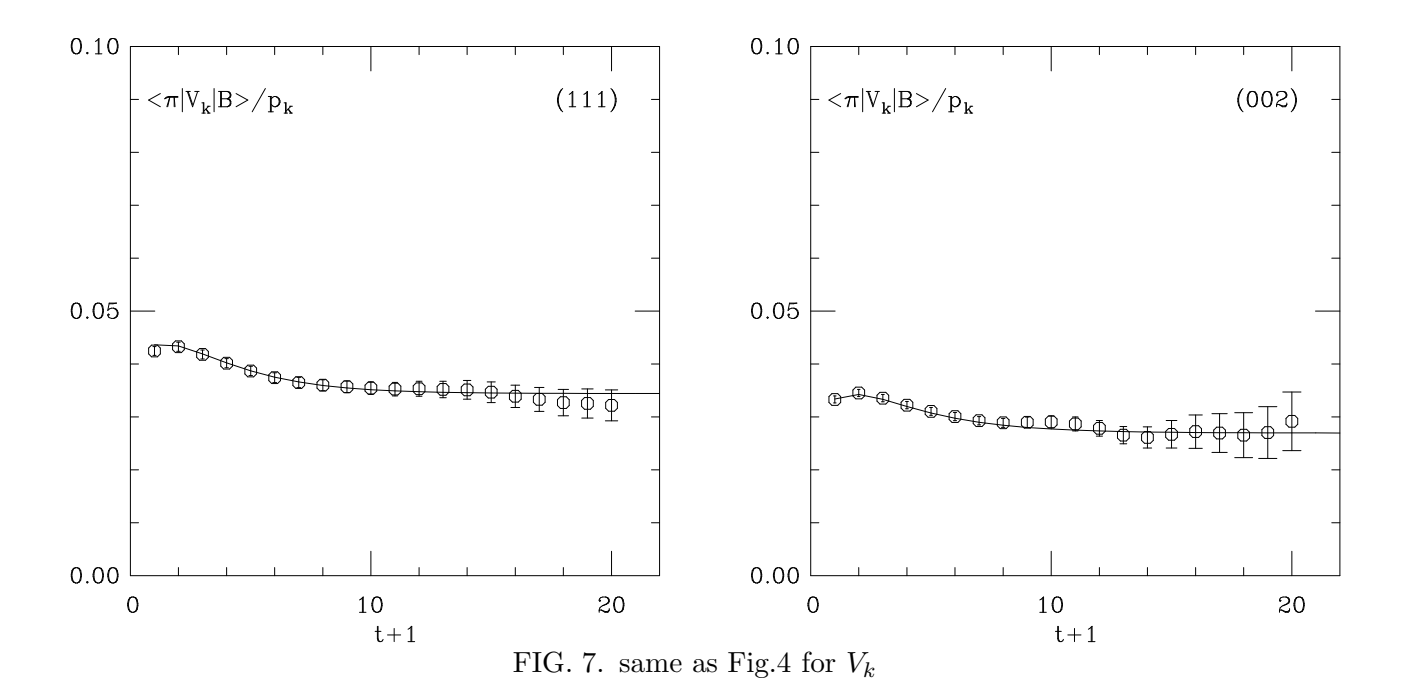


FIG. 4. Fits to 3-point correlators. All fits have 3 exponentials coming in from the left and 1 or 2 exponentials from the right. Both the fit and the data have been multiplied by  $e^{E_{\pi}^{(1)}} t e^{E_{B}^{(1)}(t_{B}-t)}$  for presentation purposes. Results are shown for strange type light quarks, i.e. for the third (middle) light quark mass out of a total of 5. In the upper right corner we show the momentum of the pion.







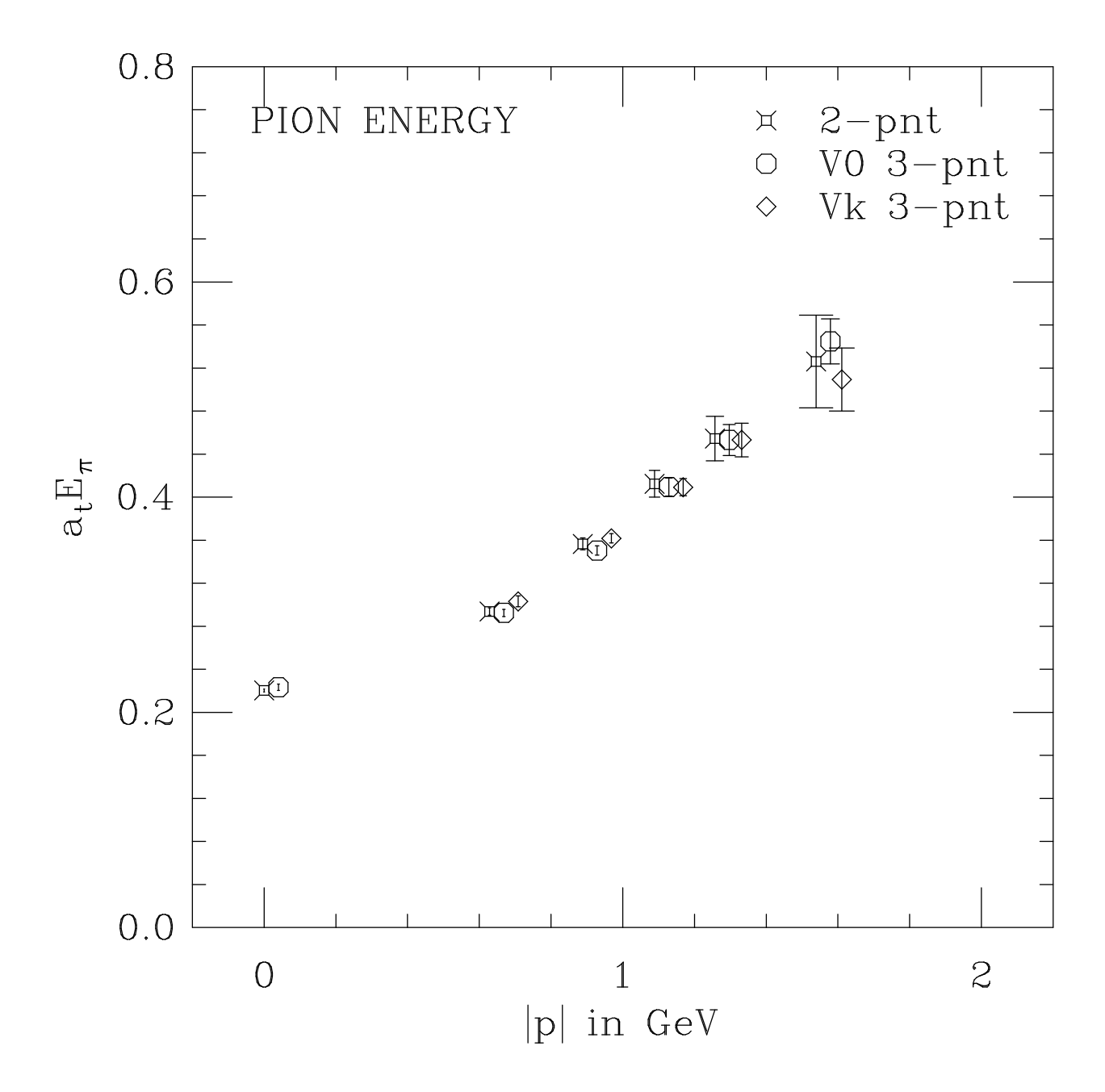
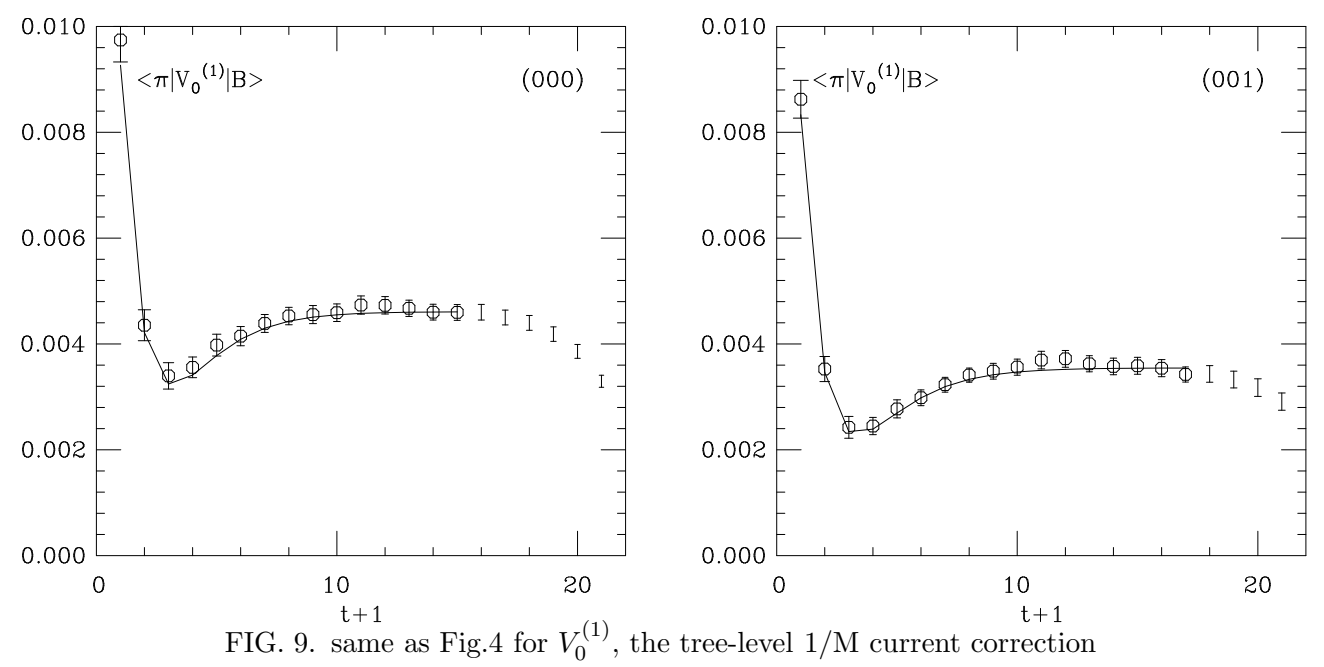
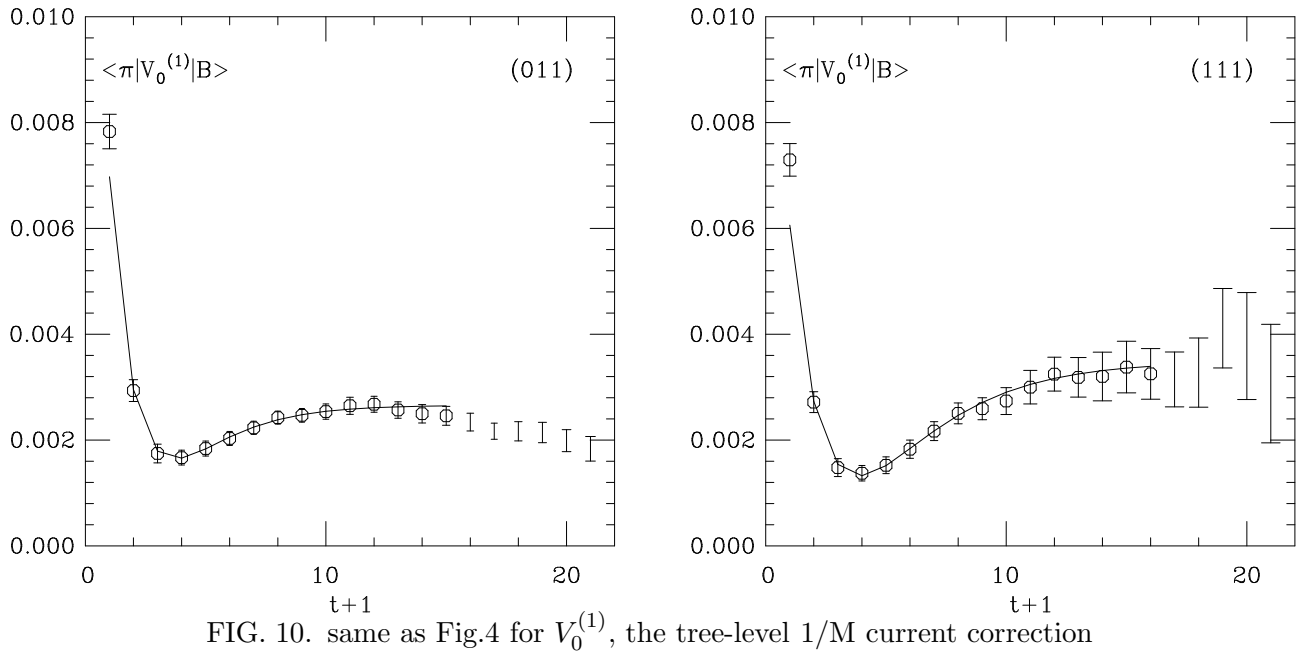


FIG. 8. Consistency test for pion energies extracted from different correlators





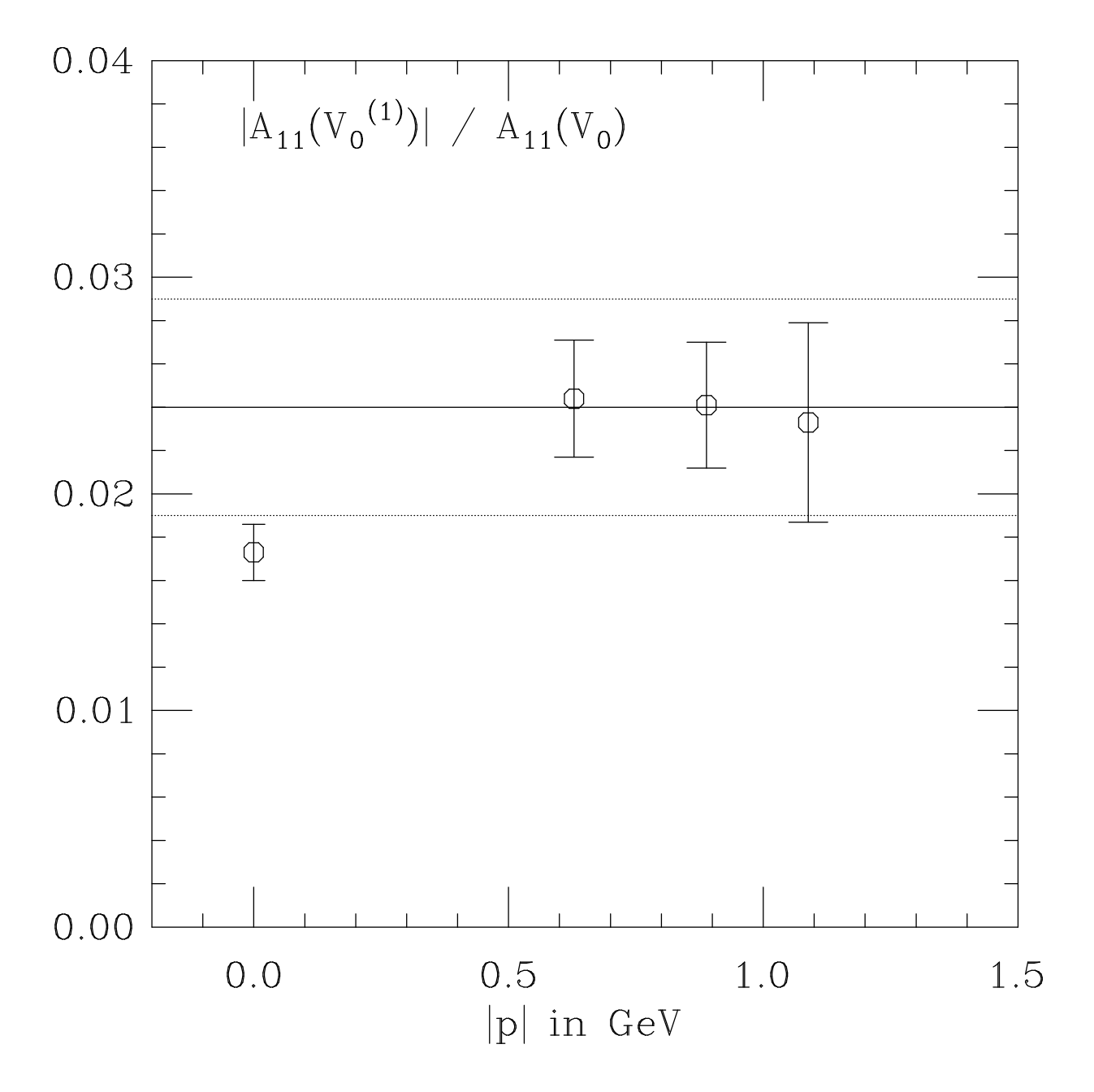


FIG. 11. Ratio of groundstate contributions to  $\langle V_0^{(1),L} \rangle$  and  $\langle V_0^L \rangle$  for several pion momenta. The horizontal line shows the one-loop  $O(\alpha_s/a_sM)$  power law subtraction term for the  $\langle V_0^{(1),L} \rangle$  matrix element.

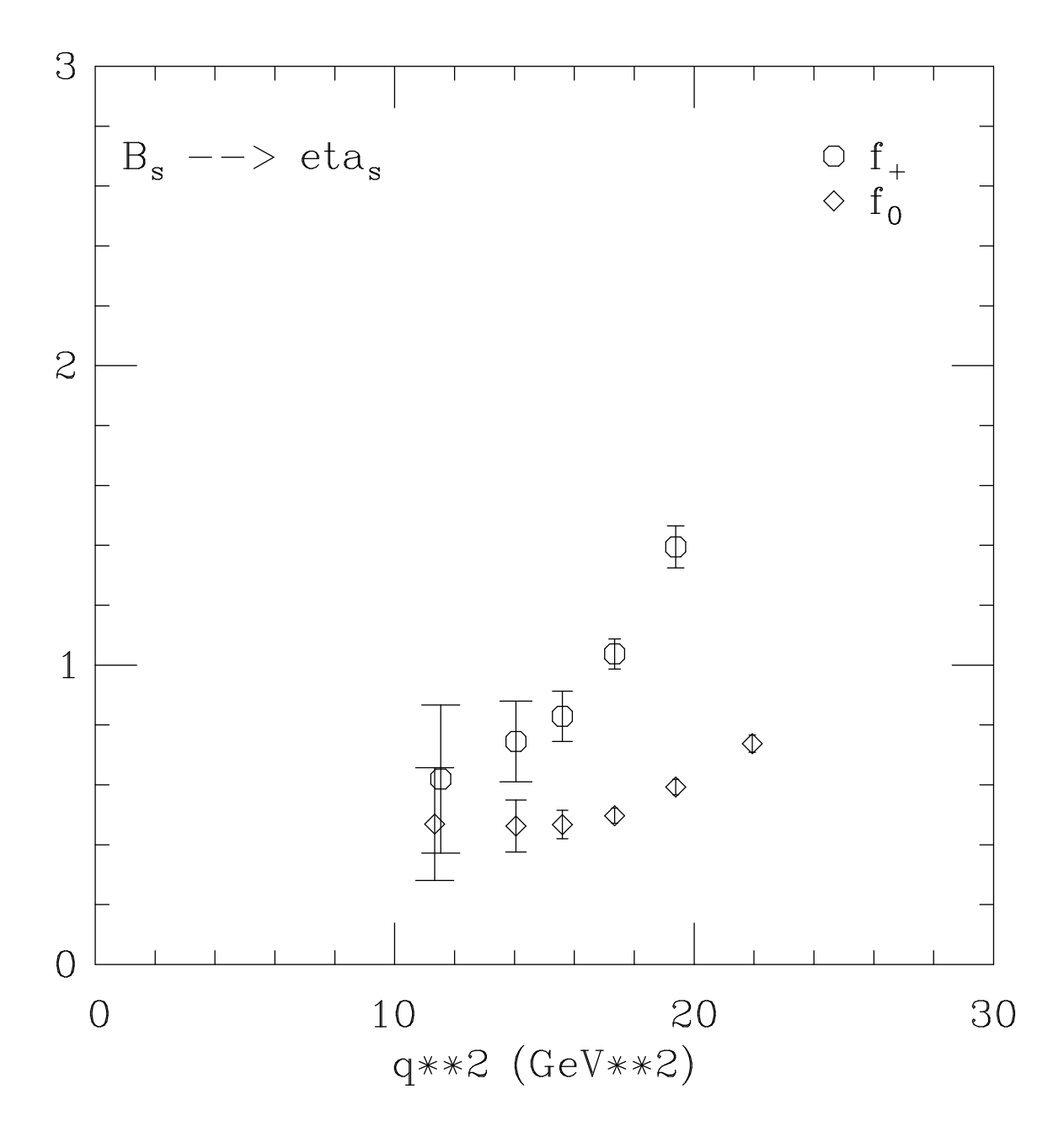


FIG. 12. The form factors  $f_+$  and  $f_0$  for the light quark mass fixed at the strange quark mass. Only statistical errors are shown.

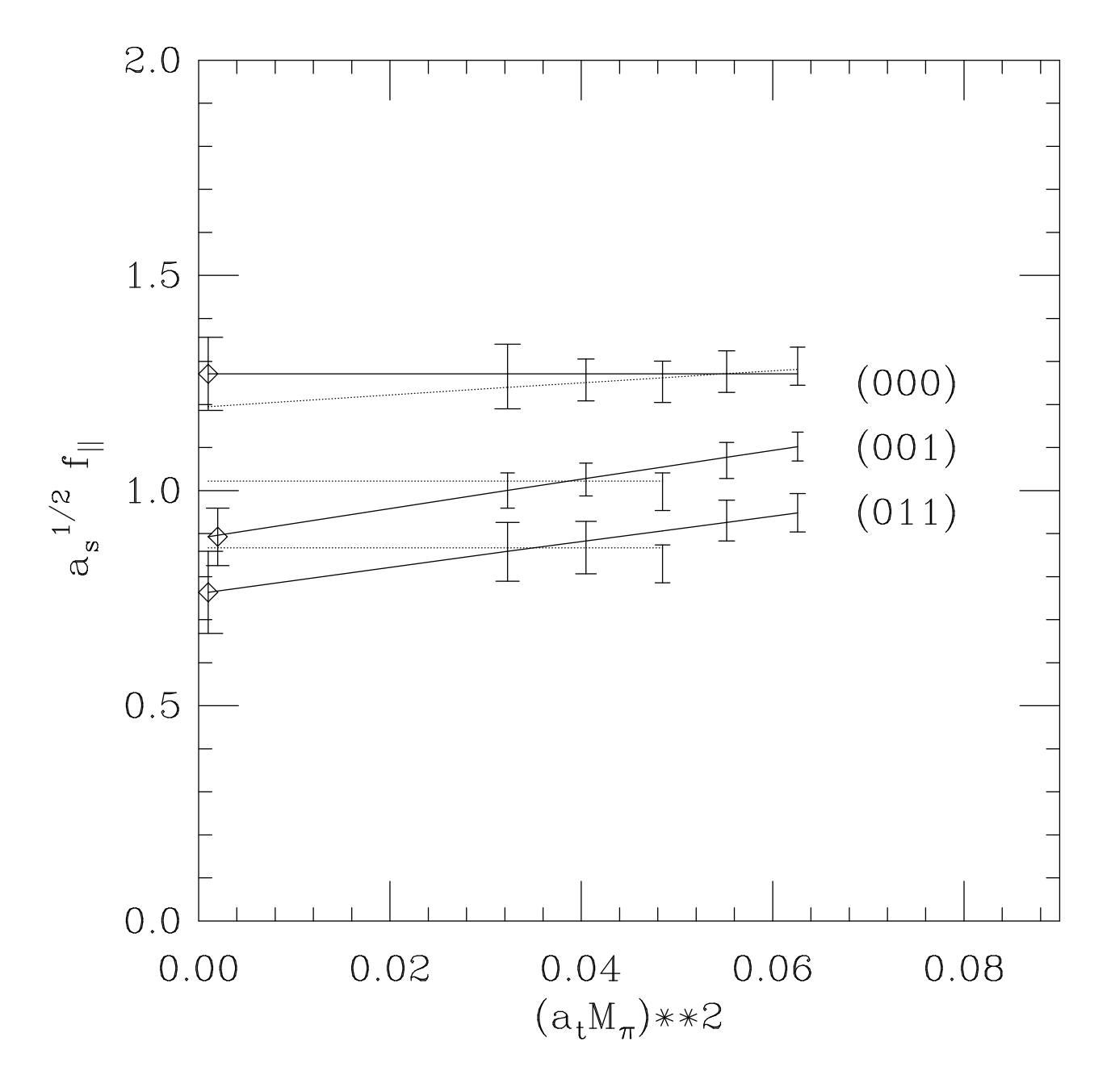


FIG. 13. Chiral extrapolations of the form factor  $f_{\parallel}$  at fixed pion momentum. Constant and linear fits were carried out to all 5 or to the last 3 data points. The full and dotted lines give some idea of spread in fit results.

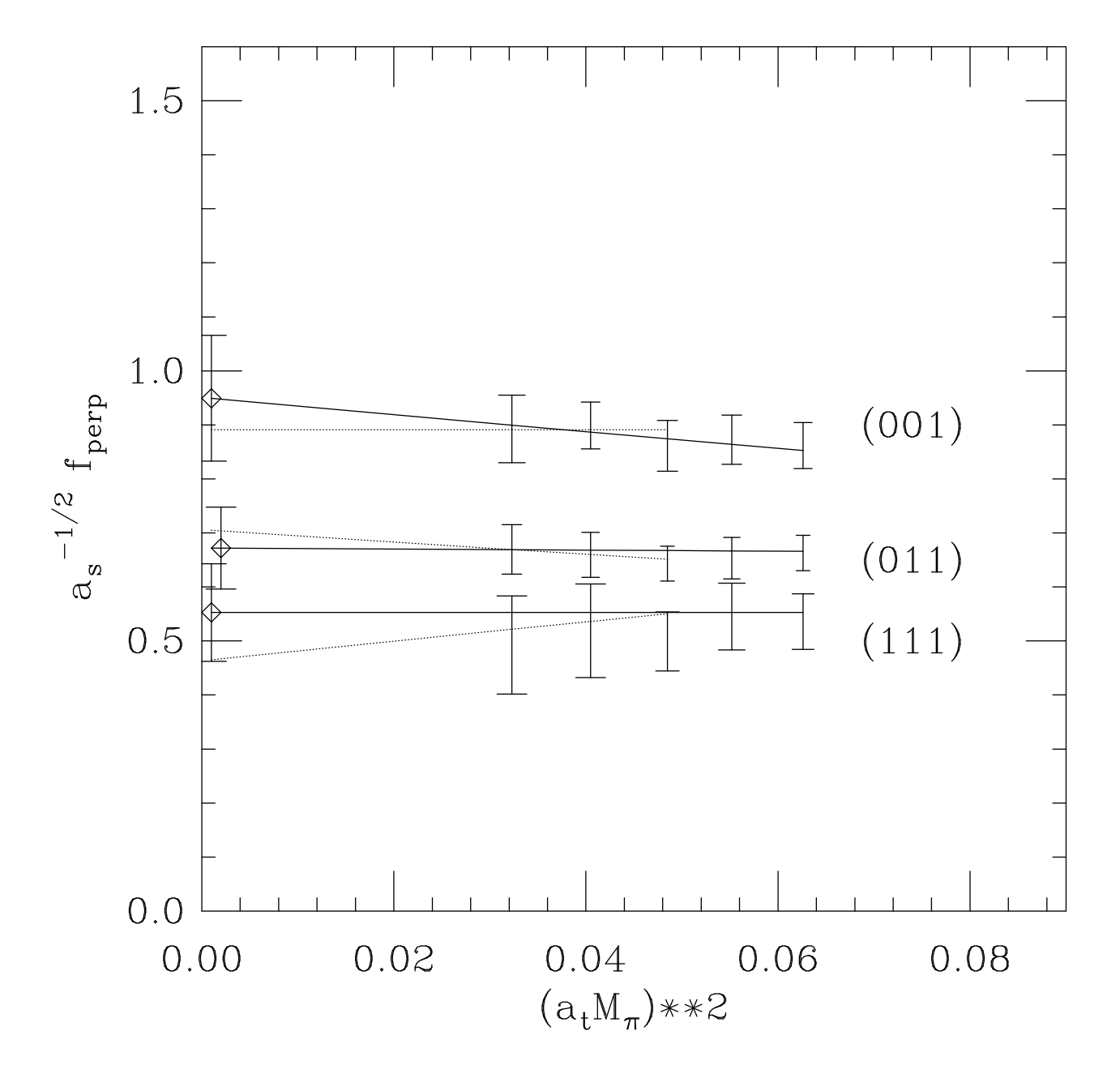


FIG. 14. Same as Fig.13 for the form factor  $f_{\perp}$ .

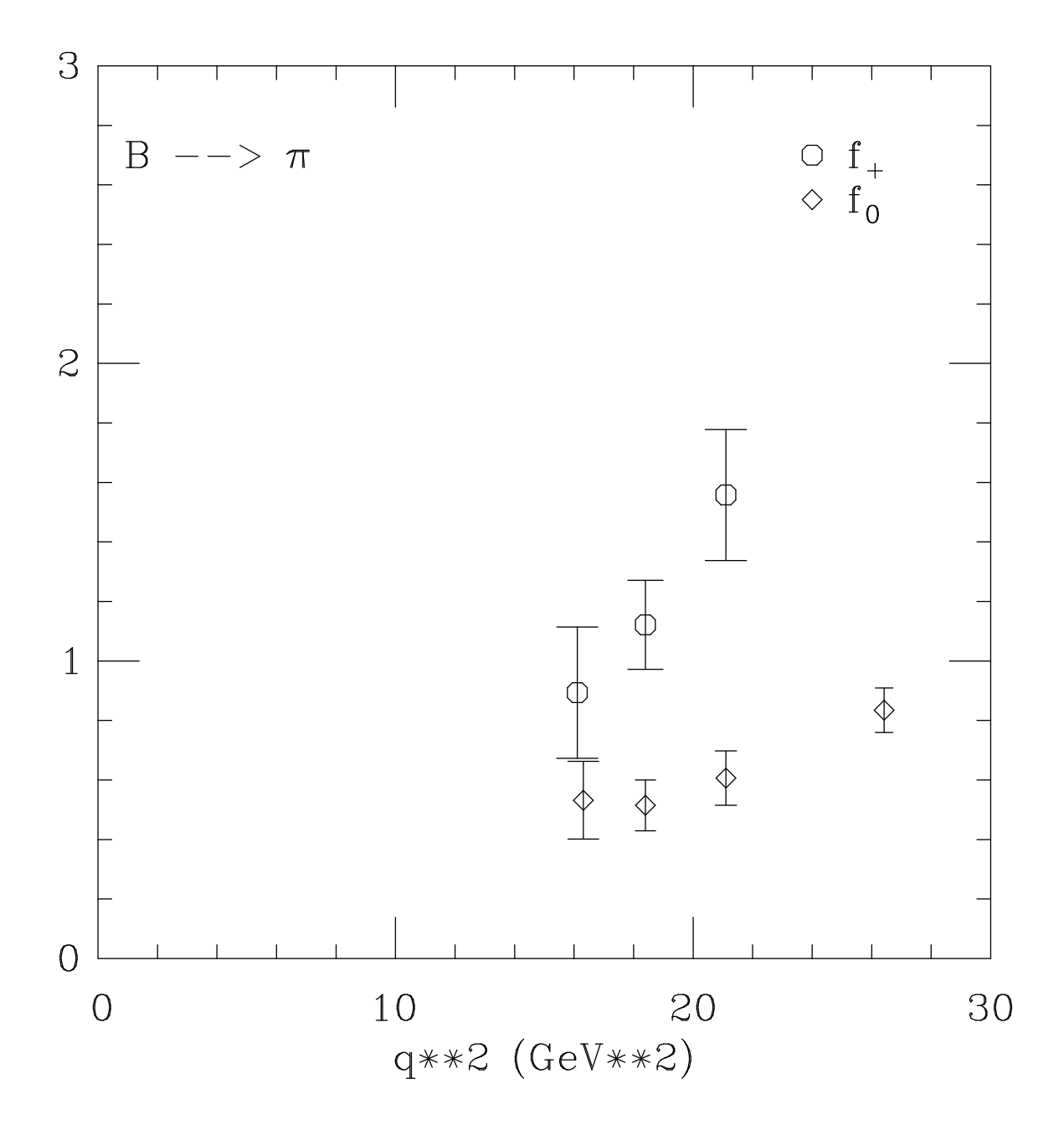


FIG. 15. The form factors  $f_+$  and  $f_0$  after chiral extrapolation to the physical pion. Statistical and chiral extrapolation errors shown.

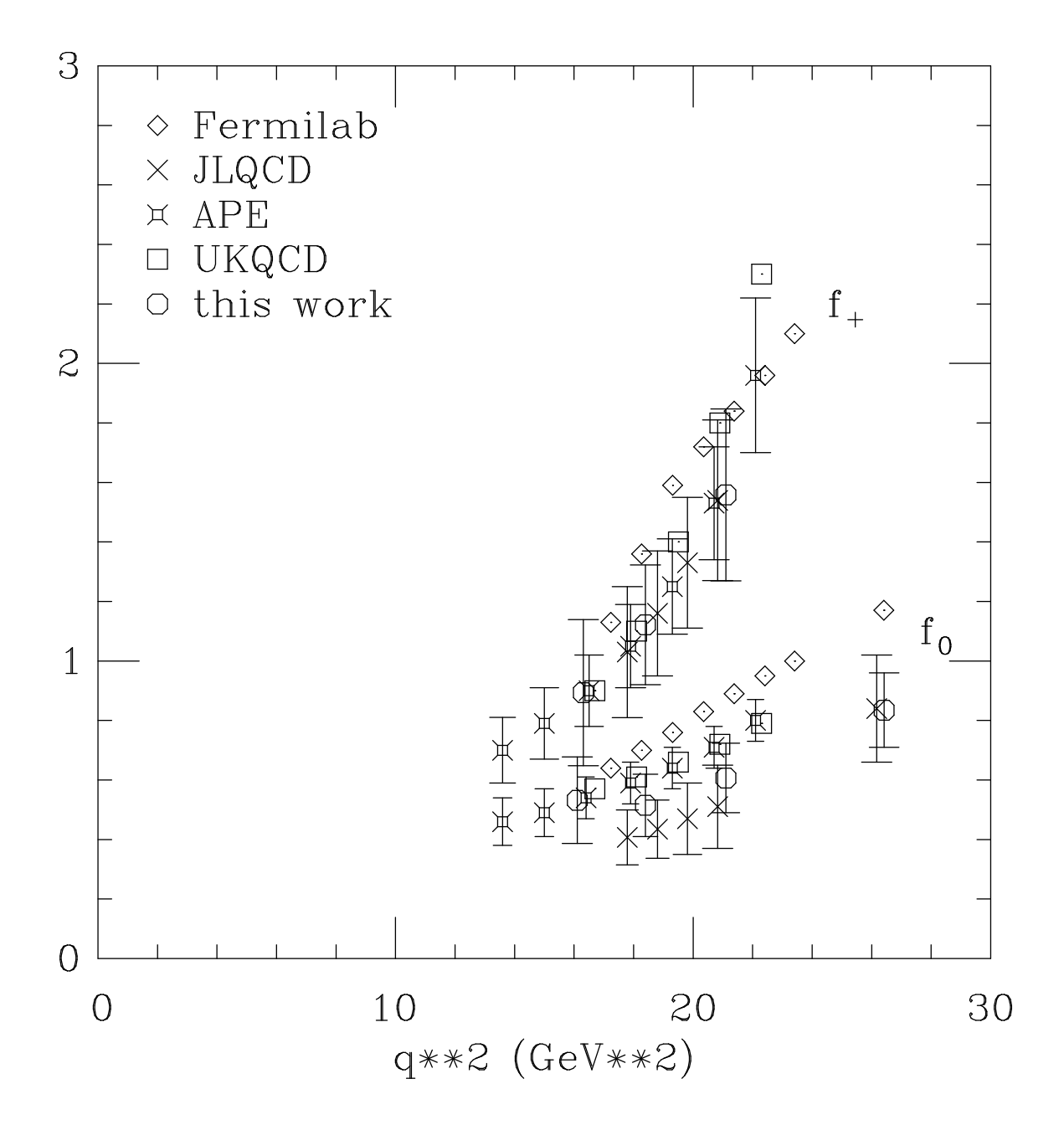


FIG. 16. Comparison with other groups. Statistical, chiral extrapolation and other systematic errors included. To avoid too much clutter we do not include errors for the Fermilab and UKQCD data points. They are comparable to those of other groups.

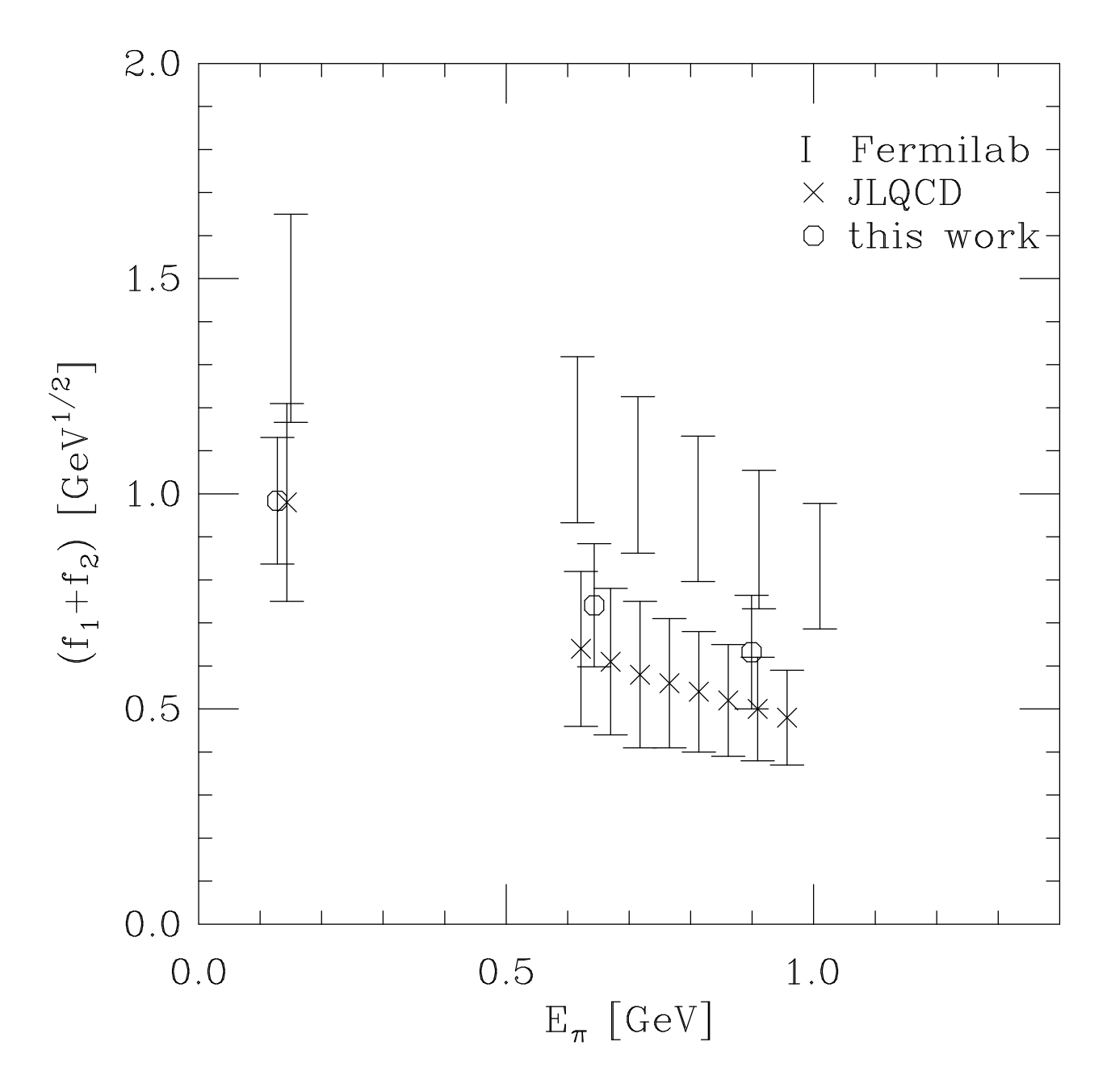


FIG. 17. Comparison with the Fermilab and JLQCD collaborations for the form factor  $(f_1+f_2)$ .

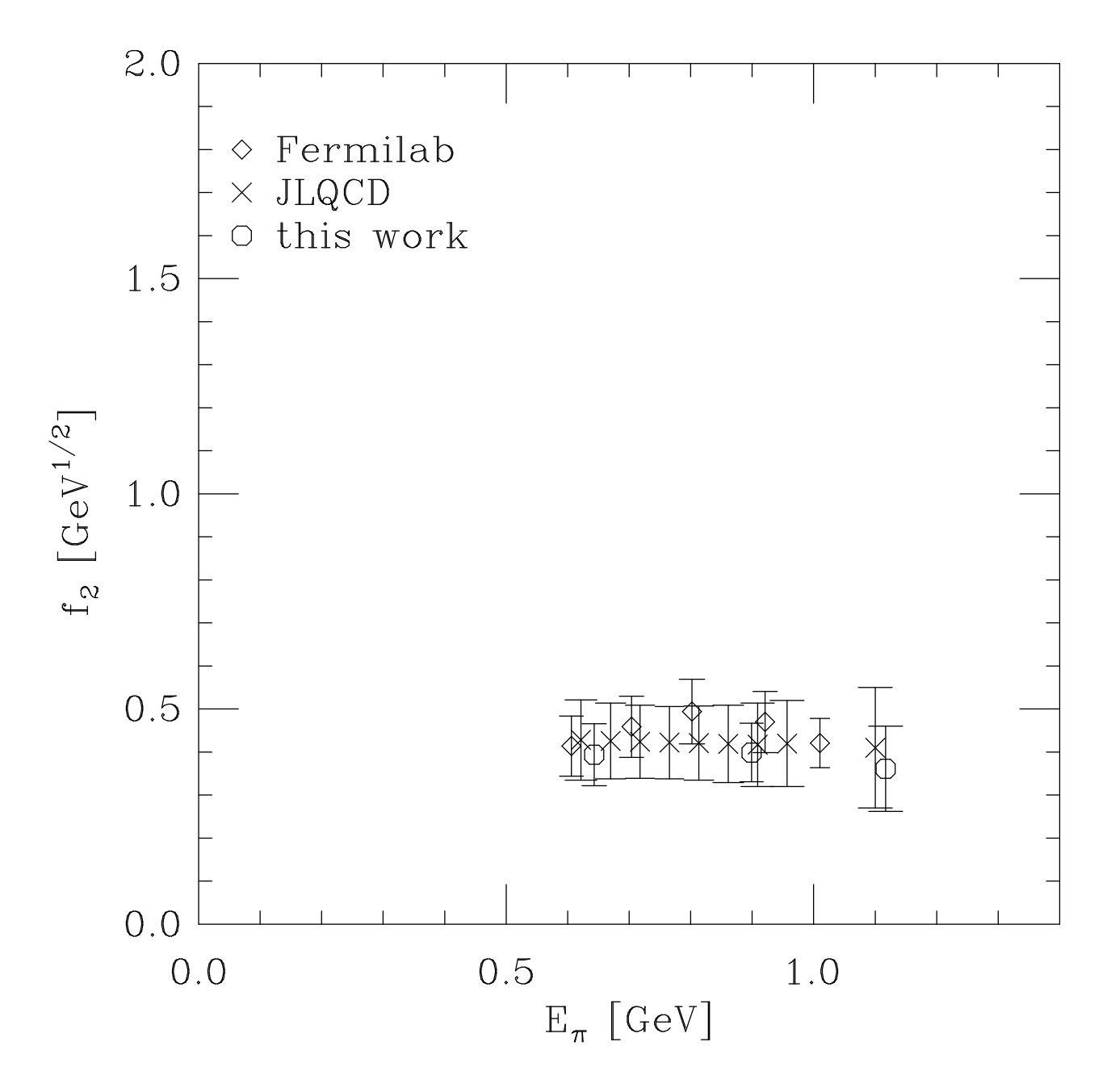


FIG. 18. Comparison with the Fermilab and JLQCD collaborations for the form factor  $f_2$ .

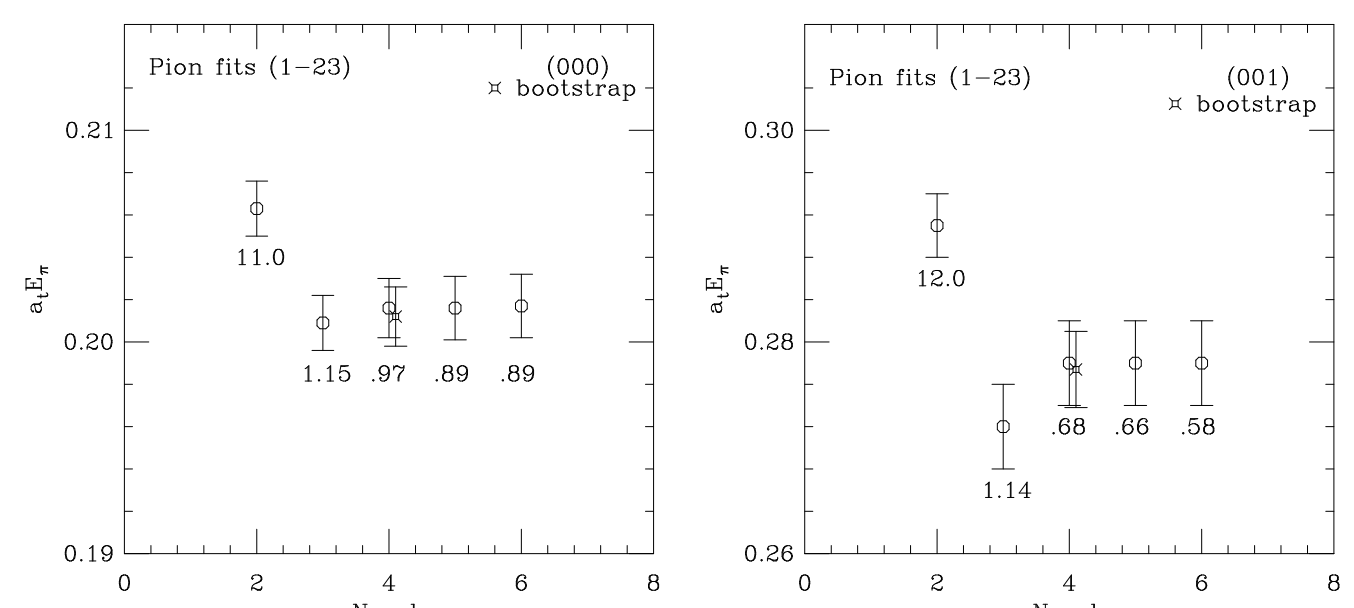
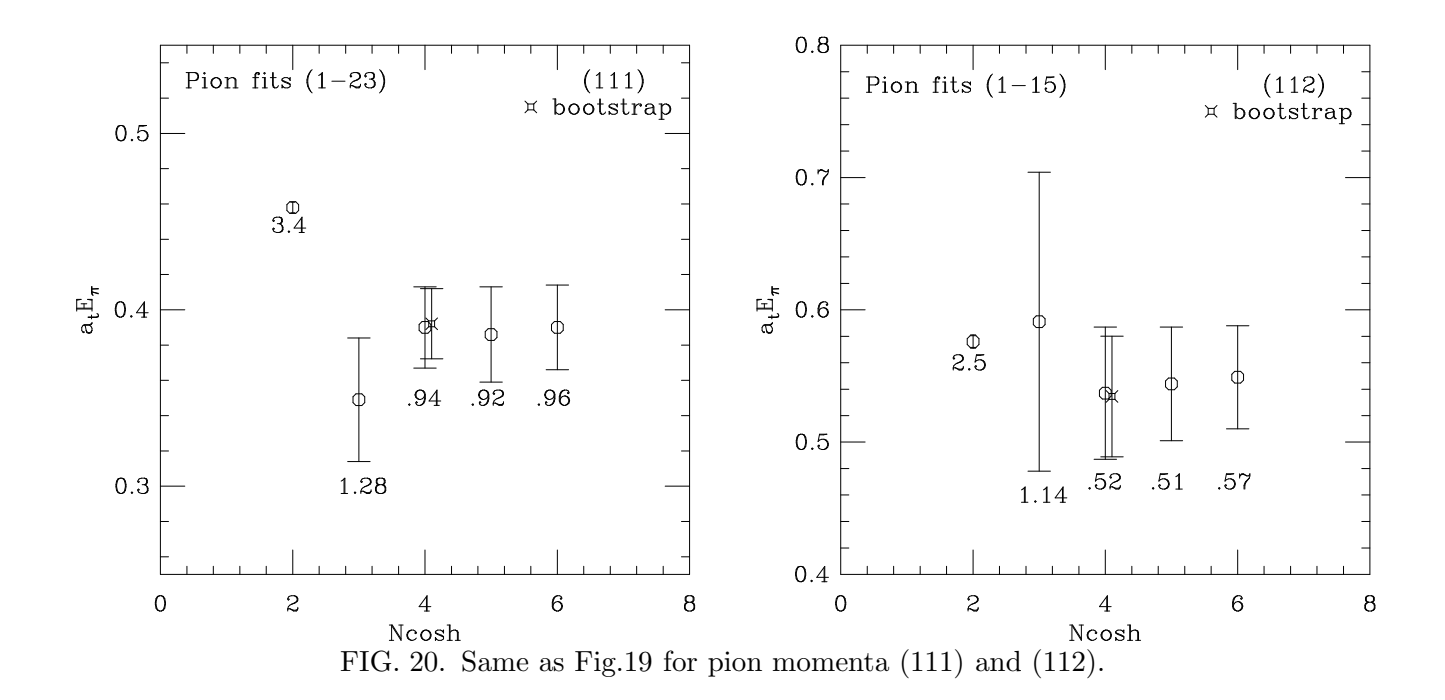


FIG. 19. Fit results for ground state pion energies versus  $N_{cosh}$ . Pion momentum is shown on upper right and the fit range on upper left corners. The fancy star shows bootstrap fit results. The numbers below data points give  $\chi^2/d.o.f$ .



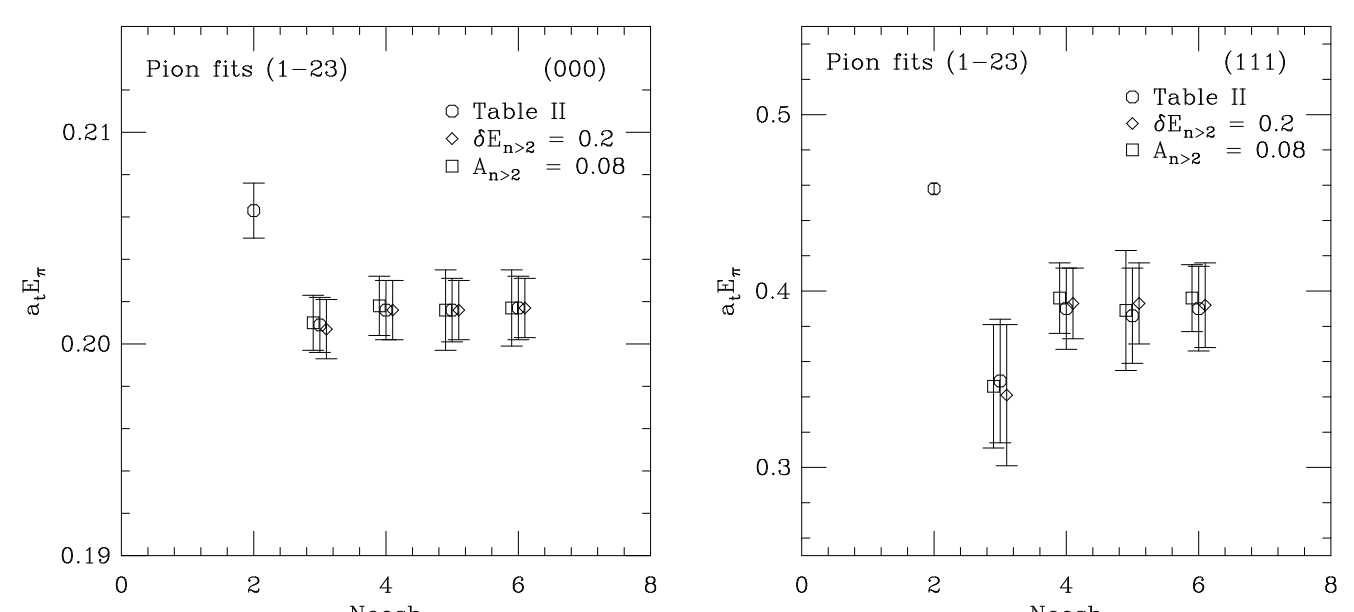


FIG. 21. Comparisons of fits using priors of Table II with fits after changing the n > 2 priors as indicated.

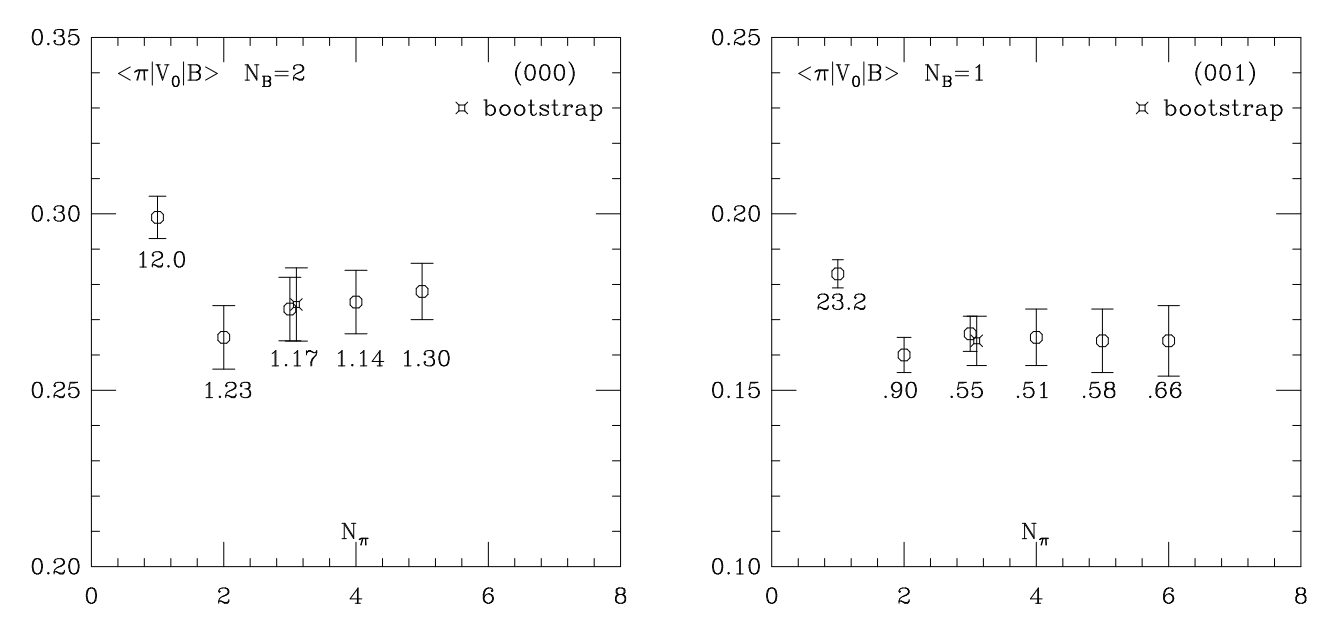


FIG. 22. Fit results for the groundstate amplitude  $A_{11}$  from the  $\langle V_0 \rangle$  threepoint correlator. The numbers below the data points give  $\chi^2/d.o.f$ .

